Materials Horizons

ROYAL SOCIETY OF CHEMISTRY

REVIEW

View Article Online
View Journal | View Issue

Cite this: *Mater. Horiz.*, 2025, **12**, 343

Graphene-based electrochemical sensors for antibiotics: sensing theories, synthetic methods, and on-site monitoring applications

Yangguang Zhu,[abd] Chen Ye,[cd] Xiao Xiao,[h] Zhuang Sun,[ad] Xiufen Li,[b] Li Fu,[e] Hassan Karimi-Maleh,[fg] Jun Chen*[h] and Cheng-Te Lin*[acd]

Received 17th June 2024,
Accepted 30th September 2024

DOI: 10.1039/d4mh00776j

rsc.li/materials-horizons

Owing to the extensive use of antibiotics for treating infectious diseases in livestock and humans, the resulting residual antibiotics are a burden to the ecosystem and human health. Hence, for human health and ecological safety, it is critical to determine the residual antibiotics with accuracy and convenience. Graphene-based electrochemical sensors are an effective tool to detect residual antibiotics owing to their advantages, such as, high sensitivity, simplicity, and time efficiency. In this work, we comprehensively summarize the recent advances in graphene-based electrochemical sensors used for detecting antibiotics, including modifiers for electrode fabrication, theoretical elaboration of electrochemical sensing mechanisms, and practical applications of portable electrochemical platforms for the on-site monitoring of antibiotics. It is anticipated that the current review will be a valuable reference for comprehensively comprehending graphene-based electrochemical sensors and further promoting their applications in the fields of healthcare, environmental protection, and food safety.

Wider impact

The key points discussed in this review include the fabrication of graphene-based electrochemical sensors for antibiotics, the theoretical underpinnings of electrochemical sensing mechanisms, and the evolution of portable electrochemical platforms for on-site monitoring. These advancements are of significant wider interest as they not only enhance our ability to detect and quantify antibiotics in various samples but also contribute to the broader fields of environmental science, public health, and materials engineering. The future is expected to be marked by further refinement of sensor technology, with a focus on improving detection limits, selectivity, and the practicality of on-site monitoring. The insights provided in this review will be instrumental in guiding future research, particularly in understanding the complex interactions at the electrode surface and the redox processes that facilitate the detection of specific antibiotics. By addressing the questions of detection performance improvement, material modification on graphene nanosheets, the underlying sensing mechanisms, and the status of equipment platforms, this review aims to clarify the current state of graphene-based electrochemical sensors for antibiotics and their readiness for real-world applications. The potential for miniaturization and portability is a critical aspect as it will enable more widespread and accessible monitoring of antibiotic residues, thus safeguarding both ecological systems and human health.

[a] *Key Laboratory of Advanced Marine Materials, Ningbo Institute of Materials Technology and Engineering (NIMTE), Chinese Academy of Sciences, Ningbo 315201, P. R. China. E-mail: linzhengde@nimte.ac.cn*
[b] *Laboratory of Environmental Biotechnology, School of Environmental and Civil Engineering, Jiangnan University, Wuxi 214122, P. R. China*
[c] *Center of Materials Science and Optoelectronics Engineering, University of Chinese Academy of Sciences, Beijing 100049, P. R. China*
[d] *Qianwan Institute, Ningbo Institute of Materials Technology and Engineering (NIMTE), Chinese Academy of Sciences, Ningbo 315201, P. R. China*
[e] *College of Materials and Environmental Engineering, Hangzhou Dianzi University, Hangzhou 310018, P. R. China*
[f] *School of Resources and Environment, University of Electronic Science and Technology of China, Chengdu 611731, P. R. China*
[g] *School of Engineering, Lebanese American University, Byblos 1102-2801, Lebanon*
[h] *Department of Bioengineering, University of California, Los Angeles, Los Angeles, CA, 90095, USA. E-mail: jun.chen@ucla.edu*

1. Introduction

Antibiotics can be utilized as revolutionary medicines for curing various infectious diseases in livestock and humans.[1–3] However, inappropriate use of antibiotics leads to the excessive release of residual antibiotics into the aquaculture industry, medications, and wastewater.[4] The accumulation of residual antibiotics in the environment produces harmful effects on nontarget organisms, and causes contamination of food and natural water resources and associated human health threats by bacterial resistance to antibiotics.[5–7] In particular, antibiotic consumption has reached over 100 000 ton and 0.7 million deaths per year related to antibiotic resistance is estimated on a global scale.[8] According to the declaration of the World Health

Organization, numerous antibiotics are identified as potential environmental contaminants and classified as furans, amphenicols, β-lactams, quinolones, macrolides, sulfonamides, tetracyclines and aminoglycosides.[9–11] For human health and ecological safety, it is urgent to monitor the residual antibiotics with accuracy and convenience.

Conventional analytical methods, such as high-performance liquid chromatography (HPLC), liquid chromatography–mass spectrometry (LC–MS), gas chromatography–mass spectrometry (GC–MS), and electrochemical detection methods, for antibiotic detection have been under development for decades.[12–15] Among them, chromatography enables the simultaneous detection of multiple antibiotics and offers advantages such as high sensitivity and strong anti-interference capability.[12,13] Yet, it still faces bottlenecks, such as costly equipment, complex sample pretreatments, and high detection costs, making it suitable only for sample analysis in laboratory research. Hence, constructing electrochemical sensors has been preferably accepted due to its high sensitivity, simplicity, and time efficiency.[16–18] However, direct electrochemical detection of antibiotics on conventional electrodes like glassy carbon electrodes (GCEs) usually confronts low sensitivity. Thus, adopting chemical modification with various nanomaterials on electrochemical electrodes has become a widely used strategy.[19–21]

Graphene is a two-dimensional nanomaterial consisting of a single layer of carbon atoms arranged in a hexagonal honeycomb lattice. Its unique atomic structure and electronic properties endow it with exceptional electrical, optical, and chemical characteristics.[22] When considering its electrochemical aspects, it has been regarded as a perfect electrode modification material due to its excellent properties, such as high surface-to-volume ratio, good electrical conductivity, favourable biocompatibility and rapid electron transferring rate.[18,23,24] Moreover, electrochemical signals can be further enhanced through the functionalization of graphene *via* covalent and non-covalent modifications.[25] Recently, graphene-based electrochemical sensors for antibiotics have been extensively constructed, and the detection performance including selectivity, limit of detection (LOD) and real sample analysis have been greatly improved.[26–28]

As far as we know, the focus of the reported reviews is on describing the status *via* bibliometric analysis and highlighting the research on graphene-based nanocomposite-modified electrodes in the context of materials science and their application in determining antibiotics in real samples within a laboratory environment.[29–34] However, it is inadequate for comprehensively reviewing graphene-based electrochemical sensors for antibiotics. The specific function of graphene with various materials in electrode fabrication is not elaborated. The antibiotic detection mechanism involved in electrochemical sensing is not clear yet, especially referring to the redox reaction process involving electron transferring and interfacial interactions between the electrode surface and the adsorbed molecules at the atomic level. Furthermore, whether the electrochemical sensors constructed in current stage achieve the requirement for the on-site monitoring of antibiotics in real samples is unknown.

In this review, we focus on three aspects: graphene-based modifiers for electrode fabrication, theoretical analyses of electrochemical sensing mechanisms, and portable electrochemical platforms for the on-site monitoring of antibiotics in real samples. It is anticipated that our review will be a valuable reference for comprehending the whole fabrication process of graphene-based electrochemical sensors, and further promoting the development of the sensors for practical applications in trace level detection of antibiotics.

2. Overview of the construction of graphene-based electrochemical sensors for antibiotics

Since 2D graphene with various forms can be fabricated in mass production, graphene-based electrochemical sensors for antibiotics have been constructed after extensive research.[35–37] Antibiotics can be classified as aminoglycosides, tetracyclines, sulfonamides, macrolides, quinolones, beta-lactams, amphenicols and furans. Their general characteristics and types of electrodes are shown in Table 1. A development timeline of graphene-based electrochemical sensors for antibiotics

Table 1 Commonly used antibiotics, their general characteristics and types of electrodes

Antibiotic class	Type	Chemical formula	Mechanism of action	Side-effects	Electrodes	Ref.
Aminoglycosides	Streptomycin	$C_{21}H_{39}N_7O_{12}$	Inhibits protein synthesis	Ototoxicity, nephrotoxicity	GO/P(NIPAm-MPTC-GMA)	38
	Kanamycin	$C_{18}H_{36}N_4O_{11}$			GO/Pt–Cu alloy/aptamer	39
Tetracyclines	Tetracycline	$C_{22}H_{24}N_2O_8$	Inhibits protein synthesis	Endocrine disruption of	rGO/Fe_3O_4/aptamer	40
	Oxytetracycline	$C_{22}H_{24}N_2O_9$		aquatic species,	GO/Au NPs/aptamer	41
Sulfonamides	Sulfamethoxazole	$C_{12}H_{14}N_4O_4S$	Inhibits folic acid synthesis	Diarrhea, vomiting	Graphene/ZnO	42
	Sulfadiazine	$C_{11}H_{11}N_3O_2S$			GO/COF	43
Macrolides	Azithromycin	$C_{38}H_{72}N_2O_{12}$	Inhibits protein synthesis	Decreased shelf-life	GO/CNTs	44
	Erythromycin	$C_{37}H_{67}NO_{13}$			Graphene/Au–Pt NPs	45
Quinolones	Ciprofloxacin	$C_{17}H_{18}FN_3O_3$	Inhibits DNA replication	Severe hepatic toxicity	rGO/Au NPs/aptamer	46
	Ofloxacin	$C_{18}H_{20}FN_3O_4$			GO/ionic liquid	47
Beta-lactams	Amoxicillin	$C_{16}H_{19}N_3O_5S$	Inhibits cell wall synthesis	Rashes, fever	GO/CdTe/Au NPs	48
	Penicillin	$C_{16}H_{18}N_2O_4S$			GO/Fe_3O_4/CNTs/aptamer	49
Amphenicols	Chloramphenicol	$C_{11}H_{12}Cl_2N_2O_5$	Inhibits protein synthesis	Inhibition of bone marrow	rGO/Co_3O_4	50
Furans	Nitrofurantoin	$C_8H_6N_4O_5$	Inhibits protein synthesis	Ecological risks, human	rGO/$GdFeO_3$	51
	Furazolidone	$C_8H_7N_3O_5$		health damage	GO/GeW	52

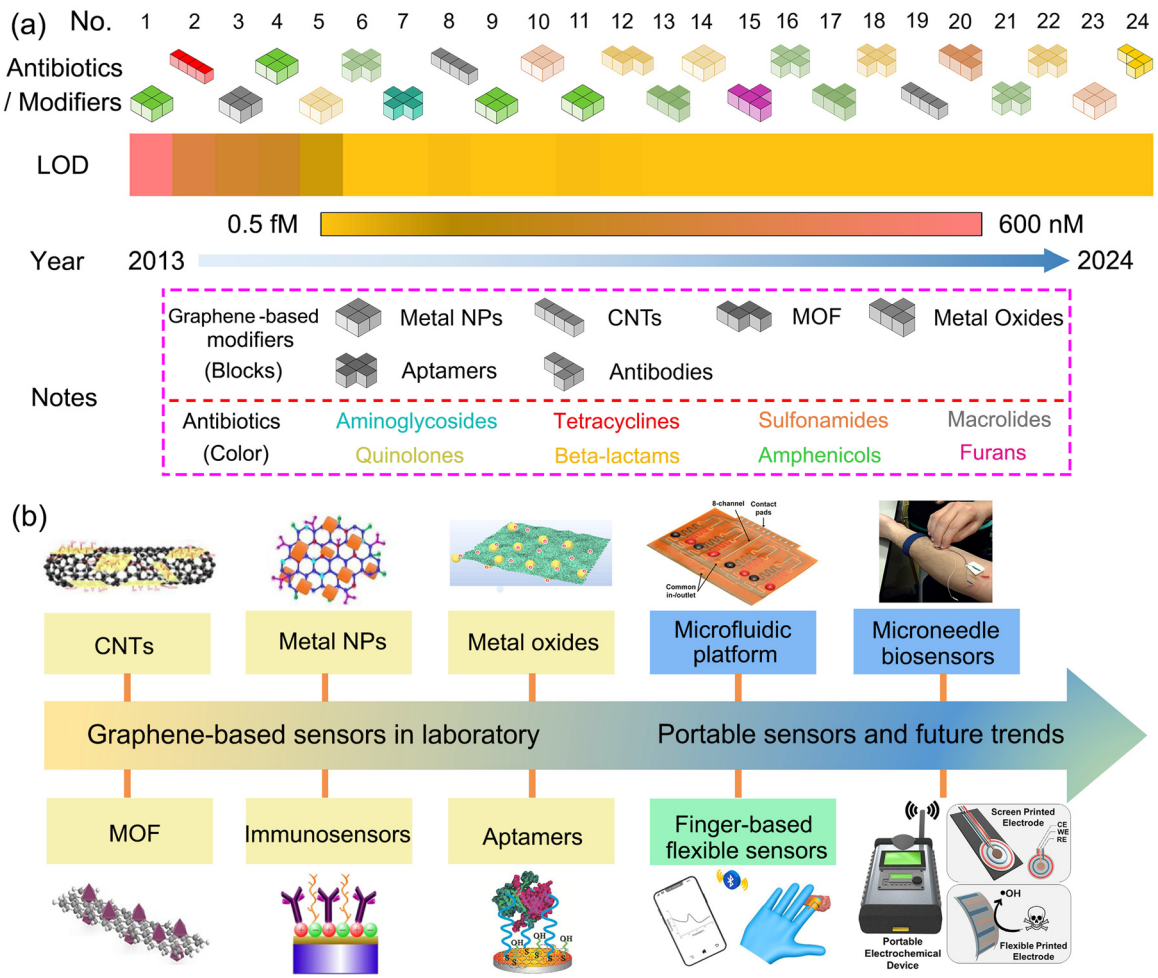

Fig. 1 Development timeline of graphene-based electrochemical sensors for antibiotics. (a) Aspects such as antibiotics, modifiers and LOD performance, and all corresponding data originate from ref. 17, 27, 46 and 53–73. (b) Evolution history of equipment platforms.[44,62,69,74–78]

including aspects as antibiotics, modifiers and LOD performance is summarized in Fig. 1a. Modifiers based on graphene can be classified as metal nanoparticles (NPs), carbon nanotubes (CNTs), metal–organic frameworks (MOF), metal oxides, antibodies and aptamers. Based on the data during the past ten decades, the distribution of antibiotic types to be detected is inhomogeneous, wherein amphenicol and aminoglycoside antibiotics occupy the majority. Hence, graphene-based electrochemical sensors for detecting other types of antibiotic molecules need to be enhanced in the future.

Aptamers or immunosensors based on graphene-modified electrodes exhibit superior detection performance towards antibiotics than other types of modifiers with a lower LOD and deserve to be further developed. The equipment platforms constructed in electrochemical sensors is essential to real applications successfully and its evolution history is depicted in Fig. 1b. Graphene-based sensors in laboratory require bulky equipment and multiple processing involved in the conventional assays, while in the contrary, potable sensors being capable of on-site monitoring indicates miniaturized device, simplified processing and wireless transmission technology, and prevails in the future.

Fig. 2a depicts the relationships between three aspects as A, B and C. Suitable modifiers designed for electrode fabrication

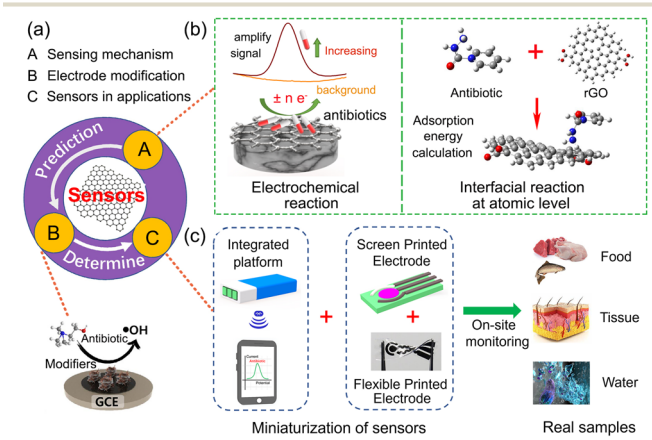

Fig. 2 Schematic of key review elements involved in graphene-based electrochemical sensors for antibiotics. (a) Relationship between the above-mentioned three aspects. (b) Electrochemical sensing mechanism in theory. Reproduced with permission.[79] Copyright from 2022, American Chemical Society. (c) Miniaturized sensing devices for on-site monitoring in real-time applications.

exhibit superior detection performance, and their upper limit was determined by real-sample analysis in this work. Conversely, the interpretation of sensing mechanism provides theoretical prediction of suitable modifiers for specific antibiotics. The sensing mechanism for antibiotics includes two parts: electrochemical reaction and interfacial reaction at the atomic level, as presented in Fig. 2b. Fig. 2c illustrates the miniaturization of sensors containing an integrated platform and screen-printed electrodes for on-site monitoring in real applications. The three aspects as A, B and C will be comprehensively discussed in the further sections.

3. Theoretical analyses of electrochemical sensing mechanism

Electrochemical sensing signal is produced by the electron transfer of analytes *via* a redox reaction on the modified electrode, which is usually proportional to the analyte concentration in practical detection.[29] The interpretation of antibiotic sensing mechanism theoretically is more important for pursuing excellent detection performance by various electrochemical techniques. Here, the antibiotic sensing mechanism includes two parts: the analysis of electrical responses at the electrochemical level, and the redox reaction process involving electron transferring and interfacial interactions between the electrode surface and the adsorbed molecules simulated by density functional theory.[80,81]

3.1 Electrochemical reaction mechanism

The principle of electrochemical antibiotic sensors is based on sensing signals generated by the redox reaction of antibiotics on the surface of graphene-based modifiers and converted into identifiable electrical signals proportional to the concentrations of antibiotics.[82] The sensing electrical signal was detected using various electroanalytical techniques such as cyclic voltammetry (CV), differential pulse voltammetry (DPV), electrochemical impedance spectroscopy (EIS) and chronoamperometry (*i*–*t*). To construct optimal electrochemical sensors for specific antibiotic detection, three key aspects including electrode modification, sensors in real-time applications and sensing mechanism will be fully discussed. The operation modes of electrochemical sensors for antibiotics are schematically illustrated in Fig. 3a.

The electrical signals produced from different electrochemical detection models show a large difference due to the different construction designs of the sensing system.[51,69,83] Through the review of the above-mentioned electrochemical sensors for antibiotics, two types of electrochemical detection models can be summarized as a direct reaction model and an indirect reaction model, as shown in Fig. 3b and c. Notably, the choice of electrochemical sensors depends on the properties of the target substance, leading to varying applicability of the two principles. For antibiotics containing structural components that readily participate in redox reactions, such as furazolidone and sulfamethoxazole, the direct model is appropriate for the detection. Conversely, for target antibiotics that exhibit

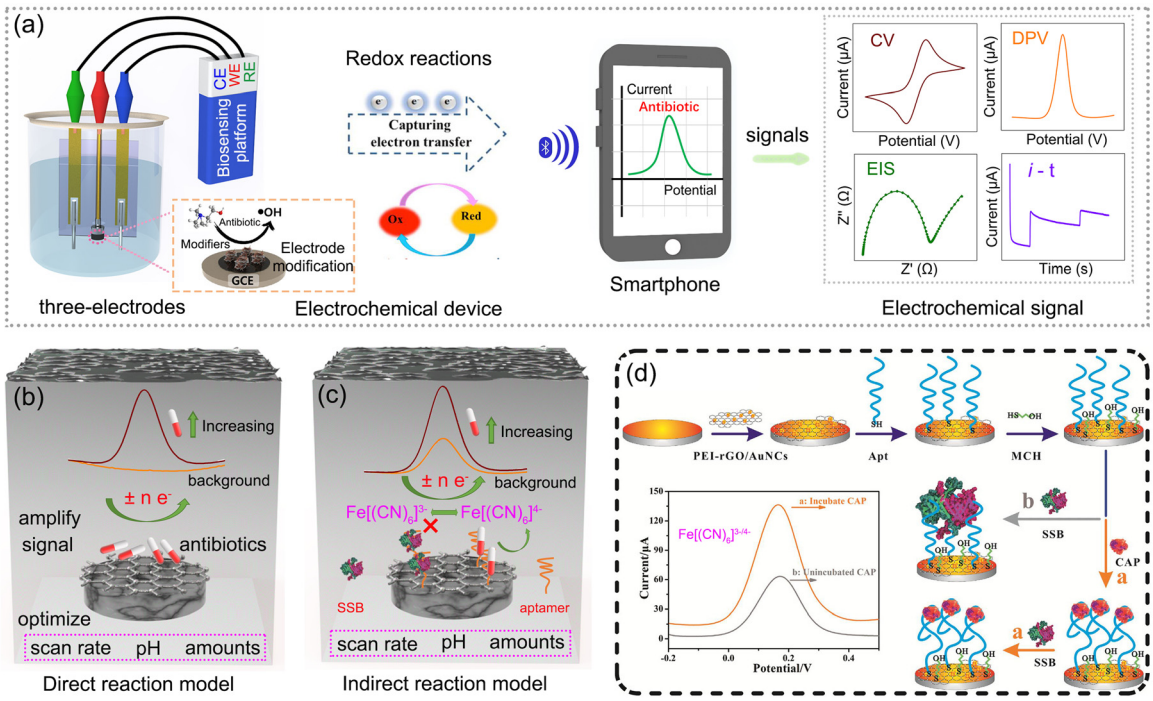

Fig. 3 Working mechanism of electrochemical sensors for antibiotics: (a) electrochemical operation modes. (b) and (c) Scheme of direct reaction model and indirect reaction model. (d) Scheme of electrochemical aptasensor for chloramphenicol (CAP) detection. Reproduced with permission.[69] Copyright from 2021, Elsevier.

difficulty in catalytic redox reactions, such as streptomycin and tetracyclines, the indirect model is the alternative option.

The electrical signals produced in the direct model are based on the direct catalytic reaction of antibiotics and enhanced with the increased concentrations of antibiotics. Through the optimization of parameters such as scan rate, pH, and amounts of modified materials, the electrochemical performance of the electrode modified for antibiotic detection is adjusted to the maximum. Then, the electrochemical redox reaction for antibiotic detection can be concluded as, for example, the irreversible reduction of a nitro group ($R\text{-}NO_2$) of nitrofurantoin (NFT) into a phenylhydroxylamine group (R-NHOH) corresponding to an equal number of electrons ($4e^-$) and protons ($4H^+$) transferred.[51] The current responses triggered by electrochemically active $GdFeO_3$/rGO nanocomposites were enhanced with the increasing concentrations of NFT. However, the direct catalytic reduction of antibiotics consumes more energy and causes increased difficulty in the fabrication of hybrid materials with higher sensitivity.

To further improve the detection performance of antibiotics, indirect reaction models are developed based on the redox reactions of a pair of $Fe[(CN)_6]^{3-/4-}$ and the special design of aptasensors. Ascribed to the easier catalytic reactions of a pair of $Fe[(CN)_6]^{3-/4-}$ and the specific binding of aptamers and antibiotics, the electrical signals toward antibiotic detection from the indirect reaction models trigger the higher, and obtain better sensitivity than direct reaction models. Chloramphenicol is taken as a typical antibiotic for illustrating the indirect reaction model, as shown in Fig. 3d, wherein polyethyleneimine-functionalized reduced graphene oxide and gold nanocubes (PEI-rGO/AuNCs) served as the modified electrode to immobilize the aptamers.[69] The large size and negative charge of single-stranded DNA-binding protein hinder the redox reactions of $Fe[(CN)_6]^{3-/4-}$ and reduce the electrical signal drastically. When chloramphenicol is present in the electrolyte, the aptamer–chloramphenicol complex is formed, which inhibits the combination of single-stranded DNA-binding protein with the aptamer, resulting in a stronger response. Herein, the modification of PEI onto the rGO surface can be achieved *via* hydrogen bonding and electrostatic attraction, effectively anchoring it to the electrode.

In particular, due to the advantages of large specific surface area, strong interfacial charge transfer capability, good stability, and ease of functionalization, graphene is an ideal material for electrode modification, which triggers intense electrochemical responses in electrochemical sensors.

3.2 Interfacial interaction mechanism by density functional theory

Conventional experimental studies are typically carried out in laboratories, involving repeated practices that are both costly and time-consuming. Computational modelling ahead of the experiments is an alternative solution to afford valuable simulations for materials screening, design and mechanism elaboration.[84] Density functional theory (DFT) satisfies the requirement for providing the theoretical prediction of material research, gaining popularity in various domains as energy storage, battery materials, environmental catalysis and sensors.[85–88] DFT modelling is carried out using software packages such as Vienna ab initio Simulation Package (VASP), Quantum Espresso, Materials Studio, CP2K and CRYSTAL.[89] With regard to electrochemical sensors specifically, it offers valuable atomic-scale insights into the structure, properties, and performance of graphene-based nanocomposites and their interfacial interaction with adsorbed antibiotics at the atomic level.

3.2.1 Descriptors involved in DFT simulations. DFT simulations are performed with the main descriptors to analyse the structure, reactivity and interfacial interaction of antibiotics adsorbed onto graphene-based nanocomposites. To illustrate the interfacial interaction mechanism of antibiotics on electrodes clearly, the identification of active sites and chemical reactivity of antibiotic structures is the primary step.[89] The highest occupied molecular orbital (HOMO), lowest unoccupied molecular orbital (LOMO) and Fukui index are used as descriptors to explore the antibiotics' optoelectronic capabilities.[90] The HOMO is electron-rich, making it prone to electrophilic attacks. Conversely, the lack of electrons in LOMO sites indicate their vulnerability to nucleophilic attacks. The HOMO–LOMO energy gap is applied to evaluate the chemical reactivity of antibiotics, and a higher value indicates its low reactivity in electrochemical redox reactions.[91] Furthermore, Fukui indexes (f_k^+, f_k^-) can be defined as the susceptibility of nucleophilic attack (f_k^+) or electrophilic attack (f_k^-) on atom k in antibiotics from eqn (1) and (2), respectively, where $q_k(N+1)$, $q_k(N)$ and $q_k(N-1)$ represent the electronic population on the atom k of anionic, cationic and neutral species of the analyte. Fukui indexes provide a quantitative way to identify the vulnerable sites to redox reactions.

$$f_k^+ = q_k(N+1) - q_k(N) \quad (1)$$

$$f_k^- = q_k(N) - q_k(N-1) \quad (2)$$

The next is to focus on interfacial interactions between the electrode surface and adsorbed antibiotic molecules. The molecular electrostatic potential (MEP) map depicts the electrostatic potential distribution of positive and negative regions in the electrode-antibiotic system, identifying the sites for nucleophilic and electrophilic attacks.[92] Qian *et al.* used the MEP map of isoniazid and different oxygen contents of rGO to reveal interfacial interaction between graphene and target antibiotics.[79] The primary distribution of electron density on the oxygen groups of rGO created repulsive forces that prevented isoniazid from approaching the rGO sheet, resulting in worse detection performance. Notably, MEP offers an intuitive way to estimate the best sites of the system for interfacial interactions. Density of states (DOS) provides details about the chemical bonding between graphene-based nanocomposites and antibiotics, exploring the active sites and interfacial interactions from the perspective of orbital interaction.[93] A quantitative tool to evaluate the stability of antibiotics adsorbed on various graphene sensing substrates was performed by adsorption energy (E_{ad})

calculation, where the negative value indicates a spontaneous reaction involved in the adsorption process.[79] In particular, the more negative value of E_{ad} presents a stronger bond between the antibiotic and the substrate.[94] The E_{ad} value can be calculated using eqn (3), where $E_{(sub/atb)}$, $E_{(sub)}$ and $E_{(atb)}$ depict the total energies of the antibiotic-adsorbed graphene material, sensor substrate and antibiotic, respectively. Ren *et al.* studied the influence of N-doped graphene on the adsorption of phenol ions using E_{ad} calculations.[95] It revealed that N doping can alter the electronic structure of graphene and create new active sites, thereby enhancing the adsorption of target molecules.

To further investigate the type of interfacial interactions between graphene-based nanocomposites and antibiotics, the reduced density gradient (RDG) is applied using eqn (4), where $\rho(r)$ denotes the electron density.[92] The various types of interactions are discriminated by the function Sign $\lambda_2(r)\cdot\rho(r)$, where Sign $\lambda_2(r)$ indicates the sign of the electron density Hessian matrix's second eigenvalue. Herein, Sign $\lambda_2(r)\cdot\rho(r) < 0$ implies the strong attractive interactions such as hydrogen bond or halogen bond, while Sign $\lambda_2(r)\cdot\rho(r) \approx 0$ depicts the lesser attractive interactions as van der Waals (vdW) attraction and Sign $\lambda_2(r)\cdot\rho(r) > 0$ presents the strong repulsive interactions as the steric effect. Using eqn (3) and (4), we can interpret the interfacial interactions between graphene-based nanocomposites and antibiotics quantitatively, and predict the suitable electrode modifiers to the specific antibiotic theoretically. Adekoya *et al.* adopted the RDG map to determine the specific type of interfacial interactions between graphene and antibiotic cephalexin (CEX).[92] Hydrogen bonding facilitates the successful binding of CEX on GO/PEG in the [Sign $\lambda_2(r)\cdot\rho(r) < 0$] region, confirming a strong interaction between CEX and GO/PEG.

$$E_{ad} = E_{(sub/atb)} - E_{(sub)} - E_{(atb)} \quad (3)$$

$$RDG = \frac{1}{2(3\pi^2)^{1/3}} \frac{|\overline{\Delta\rho}(r)|}{\overline{\rho(r)}^{4/3}} \quad (4)$$

3.2.2 Identification of active sites and chemical reactivity of antibiotic structures. Molecular modeling in describing structural, electronic and reactivity features of molecular systems can conform to the redox mechanism of electroactive molecules.[96] Silva *et al.* performed condensed-to-atoms Fukui indexes (CAFIs) to evaluate the molecular reactivity *via* molecular modeling to illustrate the mechanism of levofloxacin oxidation.[90] The *f* indices revealed the loss of two electrons from N14 and C13 atoms of levofloxacin during its oxidation process, as shown in Fig. 4a and b. Meanwhile, the Highest Occupied Molecular Orbital (HOMO) energy study is consistent with the *f* indices, as molecules with high HOMO energy values are inclined to lose electrons and oxidize susceptibly, as depicted in Fig. 4c. Furthermore, the deprotonation probability

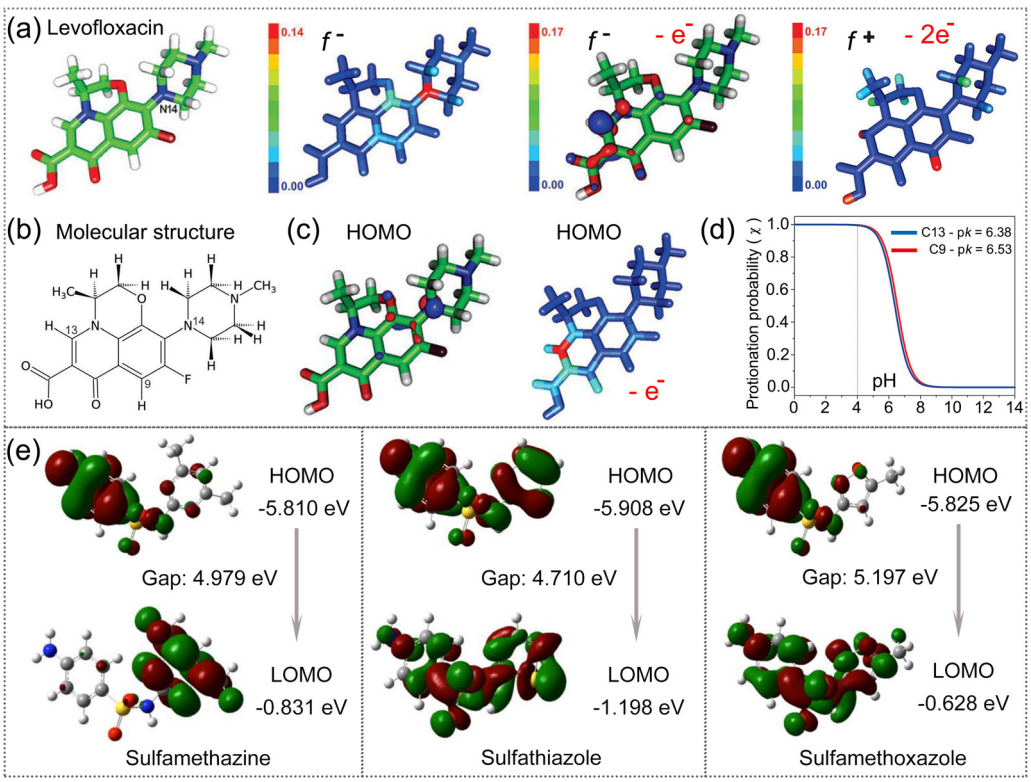

Fig. 4 Identification of active sites and chemical reactivity of antibiotic structures. (a) Illustration of the 3D structure, the lowest energy of conformation, f^- indices, (b) molecular structure, (c) HOMO distribution of levofloxacin and (d) protonation probability for C9 and C13 atoms functioned with buffer pH. (a)–(d) Reproduced with permission.[90] Copyright from 2018, Wiley-VCH. (e) HOMO, LOMO and the energy gap of sulfamethazine, sulfathiazole and sulfamethoxazole. Reproduced with permission.[91] Copyright from 2015, Walter de Gruyter.

of atoms C13 and C9 is not significant ($\chi \approx 1$), demonstrating the stability of levofloxacin after losing two electrons and revealing the oxidation mechanism of f indices, as presented in Fig. 4d. Won *et al.* explored the electronic structures and chemical reactivity of sulfonamide antibiotics and their ozone oxidation by DFT simulations.[91] The HOMO–LOMO energy gap of three antibiotics, namely, sulfathiazole, sulfamethazine and sulfamethoxazole was 4.710, 4.979 and 5.197 eV, respectively, as shown in Fig. 4e. The result revealed that sulfathiazole presents a higher reactivity than that of sulfonamide antibiotics when performed in ozone oxidation, exhibiting an effective way to discriminate the specific antibiotic conforming to modified electrodes by electroactive oxidation.

In conclusion, to assess the chemical reactivity of the target antibiotic, the HOMO–LUMO energy gap is the suitable evaluation index. A lower value indicates that the target antibiotic is highly polarizable, often exhibiting strong chemical reactivity but low stability. Fukui indexes can be further applied to identify the vulnerable sites of specific antibiotics to redox reactions.

3.2.3 Interfacial interactions of antibiotics adsorbed on graphene-based nanocomposites. The DFT method is a vital tool to evaluate the stability of antibiotic molecules adsorbed on various graphene sensing substrates, providing a chance to unveil the electrochemical interaction essence at the atomic level. Adekoya *et al.* used DFT modelling to further interpret the interaction mechanism of graphene oxide/poly(ethylene glycol) (GO/PEG) with antibiotic cephalexin (CEX), emphasizing on the adsorption sites, chemical reactivity, electrophilicity/nucleophilicity and interaction types of CEX adsorbed on GO/PEG.[92] Before analyzing the interaction, the structure of GO/PEG–CEX was optimized to unveil the most favoring adsorption site of CEX on GO/PEG, as depicted in Fig. 5a. The adsorption of CEX preferentially occurred on the edge of GO nanosheets *via* hydrogen bonding, where the H atom from carboxylic functional group of GO interacts with the N atom from the amine group of CEX. To estimate the best sites of the system for interfacial interactions intuitively, MEP was performed to discriminate electrophilic or nucleophilic attacks in the system, as shown in Fig. 5b. The negative regions are related to the

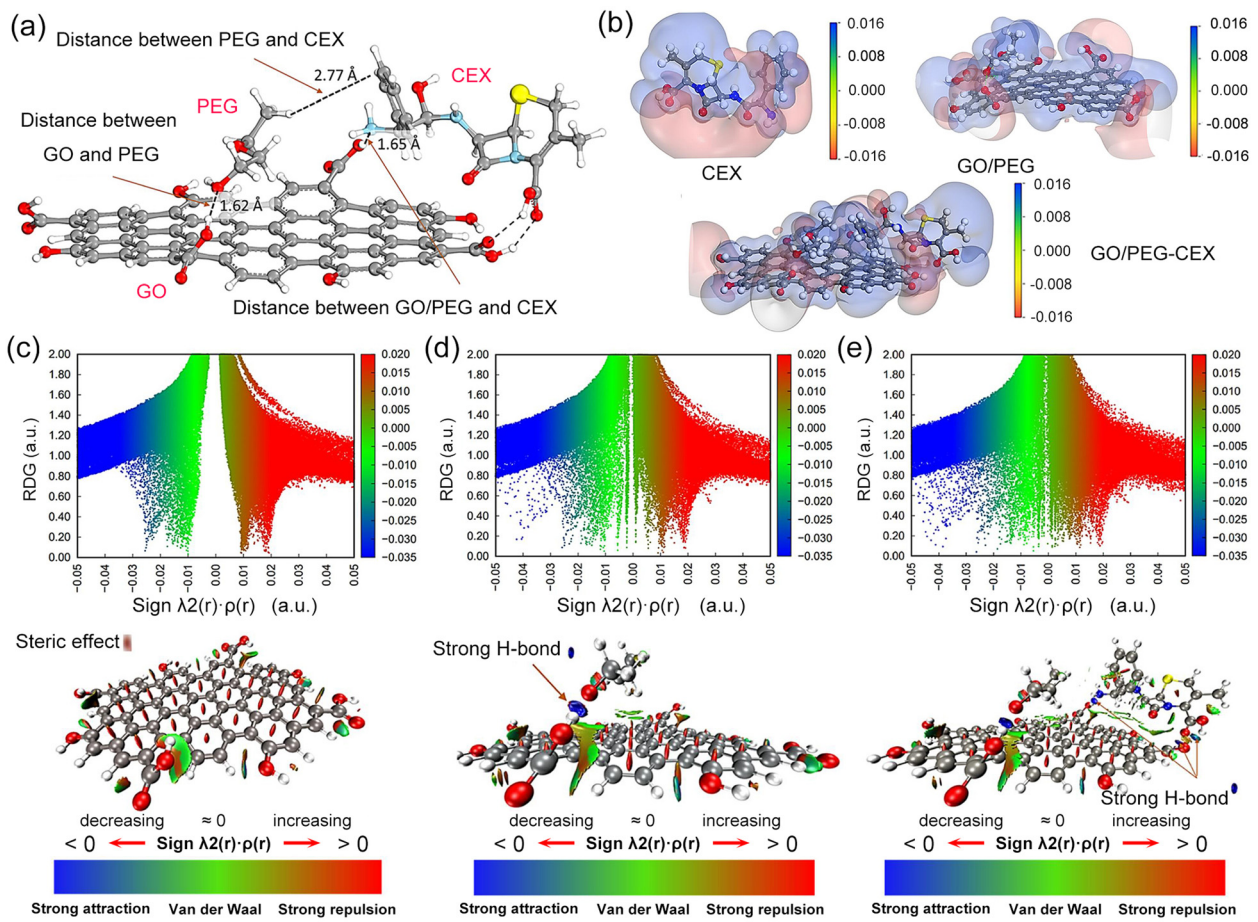

Fig. 5 Interfacial interactions of antibiotics adsorbed on graphene-based nanocomposites. (a) Optimized structure of GO/PEG–CEX. (b) MEP distribution of CEX, GO/PEG and GO/PEG–CEX. The blue regions indicate low electron density, while the red domains depict electron enrichment. RDG isosurface map for determining the type of interfacial interactions in (c) GO, (d) GO/PEG and (e) GO/PEG–CEX. (a)–(e) Reproduced with permission.[92] Copyright from 2022, American Chemical Society.

electronegative oxygen and nitrogen atoms of CEX and oxygen atoms from carboxylic functional groups of GO/PEG, which refers to electrophilicity. On the contrary, the positive regions are over the carbon and hydrogen atoms, which is related to nucleophilicity. To determine the specific type of interfacial interactions, the RDG map was applied for the analysis, as depicted in Fig. 5c–e. Hydrogen bonding enacts the successful binding of CEX on GO/PEG at three various sites, confirming a strong interaction between CEX and GO/PEG.

The influences of the electronic structure of graphene regulated by doping with elements such as nitrogen (N), varying oxygen content or hybridization with other materials are vital to elaborate the interfacial interactions of antibiotics adsorbed on graphene-based nanocomposites. Ren *et al.* investigated the influence of N-doped graphene on the adsorption of phenol ions by DFT modelling.[95] As depicted in Fig. 6a–d, the distances between the pristine rGO plane and its next to graphitic N (γ1 and γ2), pyridinic N and O atom of phenol were 2.834, 1.597, 1.508 and 2.426 Å, respectively. Compared to pristine rGO, the shorter C–O distance of N-doped rGO demonstrated that N doping can alter the electronic structure of graphene and create new active sites for enhancing the adsorption of phenol ions. The rGO plane adjacent to graphitic N presents a higher affinity for adsorbing phenol ions than pyridinic N, while pyrrolic N indicates ineffective adsorption capacity. Therefore, N doping enhances the metal-like property of graphene due to the induction of a high positive charge density on the *ortho*-carbon atoms, promoting its adsorption capacity.

Qian *et al.* conducted a DFT calculation to reveal the roles of rGO oxygen content in developing graphene-based electrochemical detection of isoniazid with high performance.[79] As shown in Fig. 6e, the positive E_{ad} of the rGO1 sensor with a higher oxygen content and isoniazid exhibited repulsive forces that prevented isoniazid from approaching the rGO sheet. Fig. 6f shows the molecular electrostatic potential of isoniazid, rGO1 and rGO2, and indicates the primary distribution of electron density on the oxygen groups to form repulsive forces. The computational results confirmed the experimental data that rGO1 behaved with weaker voltammetric responses. Osikoya *et al.* investigated the adsorption behaviour of amoxicillin on the Au/graphene electrode by DFT calculation.[93] As presented in Fig. 6g, amoxicillin presenting a vertical configuration with a

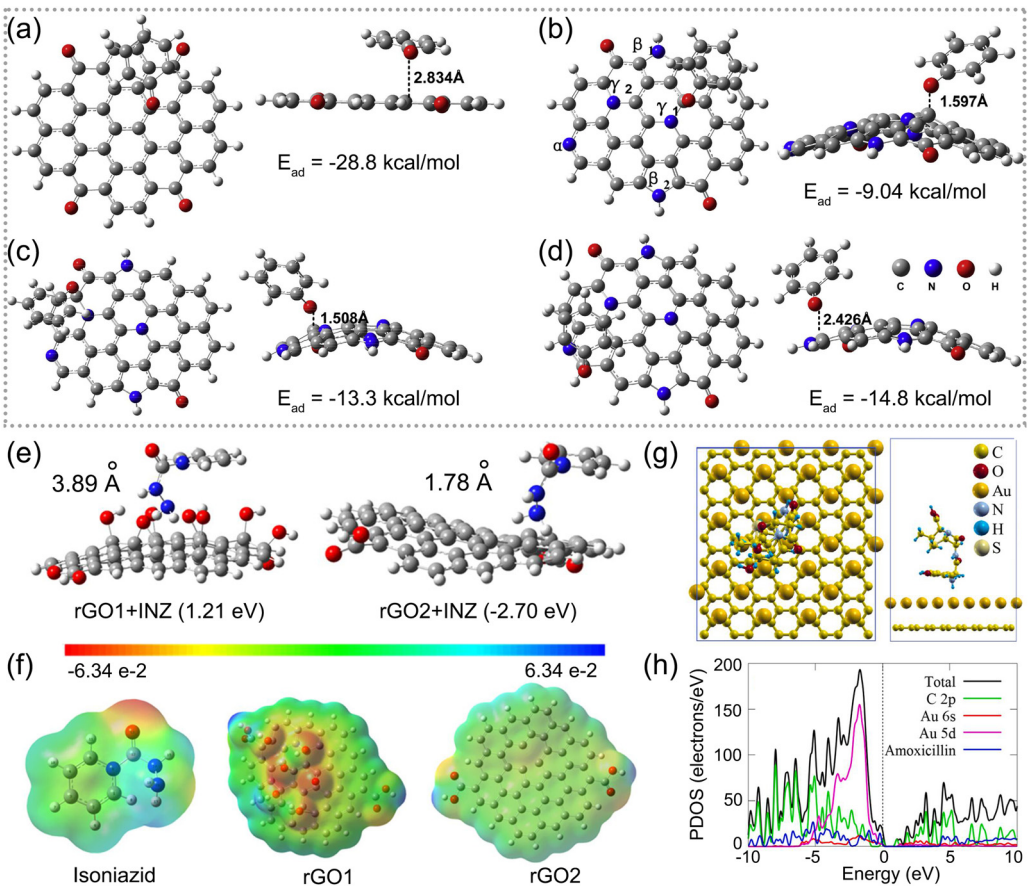

Fig. 6 Interfacial interactions of antibiotics adsorbed on graphene-based nanocomposites. Optimal models for the adsorption of a phenol ion on (a) pristine rGO and (b)–(d) various sites of N-doped rGO including three types of N as pyridinic (α), pyrrolic (β) and graphitic (γ). (a)–(d) Reproduced with permission.[95] Copyright from 2018, Elsevier. (e) Optimized structures of isoniazid adsorption on rGO1 and rGO2. (f) Molecular electrostatic map of isoniazid, rGO1, and rGO2. (e) and (f) Reproduced with permission.[79] Copyright from 2021, American Chemical Society. (g) Illustration of low-energy adsorption of amoxicillin onto the Au/graphene surface. (h) Total density of states (DOS) and partial density of states (PDOS) contributed by the Au/graphene electrode and amoxicillin. (g) and (h) Reproduced with permission.[93] Copyright from 2021, Elsevier.

–NH_2 group preferred to be adsorbed stably onto the Au/graphene electrode surface, with an E_{ad} value of −2.03 eV. The adsorption behaviour can be attributed to the formation of a strong X–H···Au (X = C or N) interaction between the Au atom and the –CH_3 or –NH_2 group of amoxicillin. Partial density of states results presented in Fig. 6h suggest that amoxicillin has a high affinity towards the Au/graphene nanointerface.

In summary, the adsorption of the target antibiotic preferentially occurred on graphene-based nanocomposites *via* hydrogen bonding, electrostatic interaction or covalent bonding. Carboxylic, epoxy or hydroxyl functional groups are the common adsorption sites on graphene-based electrodes for targeting antibiotics that contain a –CH_3 or –NH_2 group. The abundant oxygen functional groups on graphene preferentially facilitate the adsorption of target antibiotic stably through various interfacial interactions.

4. Synthesis of graphene-based modifiers for electrode fabrication

The derivative graphene is widely used as pristine graphene, graphene oxide (GO), and reduced graphene oxide (rGO), exhibiting various attributes with various forms and structures, as shown in Fig. 7a. Pristine graphene comprises carbon atoms arranged in a planar hexagonal lattice, producing excellent electronic and mechanical properties.[22] Unfortunately, it still suffers difficulties in bulk production, water dispersion and isolation, hindering its further application in sensing areas.[97] The GO surface is loaded with oxygen-containing moieties such as peripheral carboxylic acid (–COOH), in-plane epoxide (–O–) and hydroxyl (–OH) groups, possessing the stronger colloidal stability, hydrophilicity and chemical surface modification.[98] However, considerable defect density resulting from oxygen functional groups in GO decreases its electrochemical conductivity up to an electrical insulator, which is weak to sensing applications. rGO, reduced oxygen content from GO, exhibits superior electrical conductivity.[30] Yet, removing oxygen groups results in less hydrophilicity and difficulty in water dispersion to fully absorb antibiotics. To develop practical applications of graphene based on its superior physical/chemical properties, the investigation of mass-production methods compatible with the industry standard is highly demanded. The state-of-the-art synthesis approaches include Hummers' method, mechanical exfoliation in the liquid phase, and chemical vapor deposition (CVD), with the tunability of lateral size, crystallinity, and price for their own applications.[99]

As graphene's electrocatalytic activity is restricted, the functionalization of graphene is considered the effective way to facilitate its applications further and is classified as covalent and non-covalent modification, as illustrated in Fig. 7b. Covalent modification can be achieved by forming amide and carbamate ester bonds with the carboxyl and hydroxyl groups, and non-covalent modification includes weak van der Waals forces, π–π stacking, and electrostatic interaction.[25,101,102] A series of materials such as metal NPs, metal oxides, enzymes, aptamers and others are applied as modifiers to combine with graphene and fabricate electrodes to form electrochemical sensors for antibiotics.[64,68,93,103,104] Our reviewing in this part focuses on the prevalent methods to fabricate various graphene-based hybrid structures and the relationship between material structure and sensing performance, providing valuable references for the synthesis of graphene-based modifiers for electrode fabrication.

4.1 Solution blending method

Solution blending is the universal and cost-effective method to prepare graphene-based hybrids based on weak van der Waals forces and π–π stacking. Zhu *et al.* fabricated $Ti_3C_2T_x/TiO_2$ NPs by *in situ* oxidation of $Ti_3C_2T_x$/nanosheets in a controllable manner and used a small amount of rGO (<2.5 wt%) as a conductive additive to blend with $Ti_3C_2T_x/TiO_2$ NPs to form $Ti_3C_2T_x/TiO_2$ NPs/rGO heterojunction electrodes, as illustrated in Fig. 8a.[105] The rGO served as an electrically conductive cross-linked network, optimizing the interfacial structure to facilitate electron transfer. Zhu *et al.* prepared TiO_2 nanosheets (NSs) by

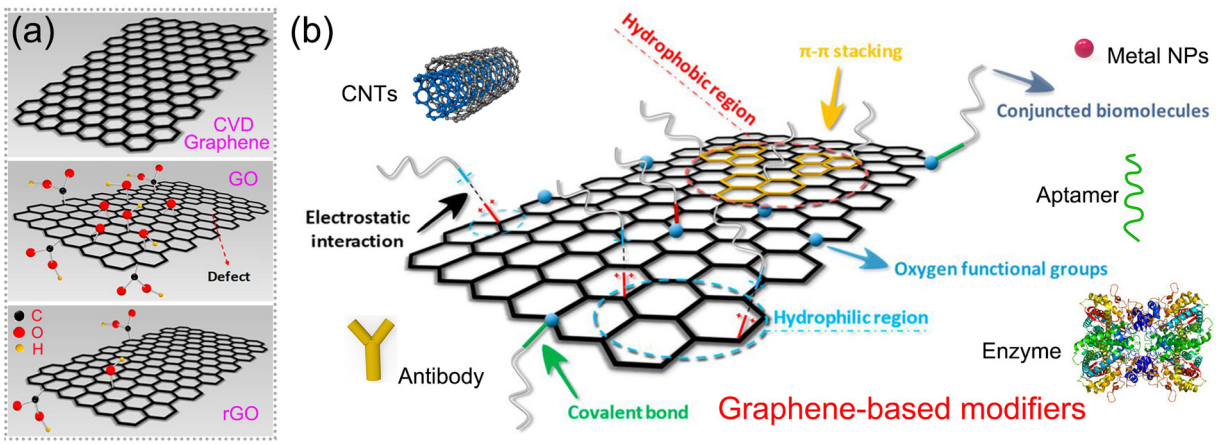

Fig. 7 Surface functionalization/decoration of graphene: (a) graphene and its derivatives. (b) Schematic of various modifiers functionalized on graphene. Reproduced with permission.[100] Copyright from 2019, Multidisciplinary Digital Publishing Institute.

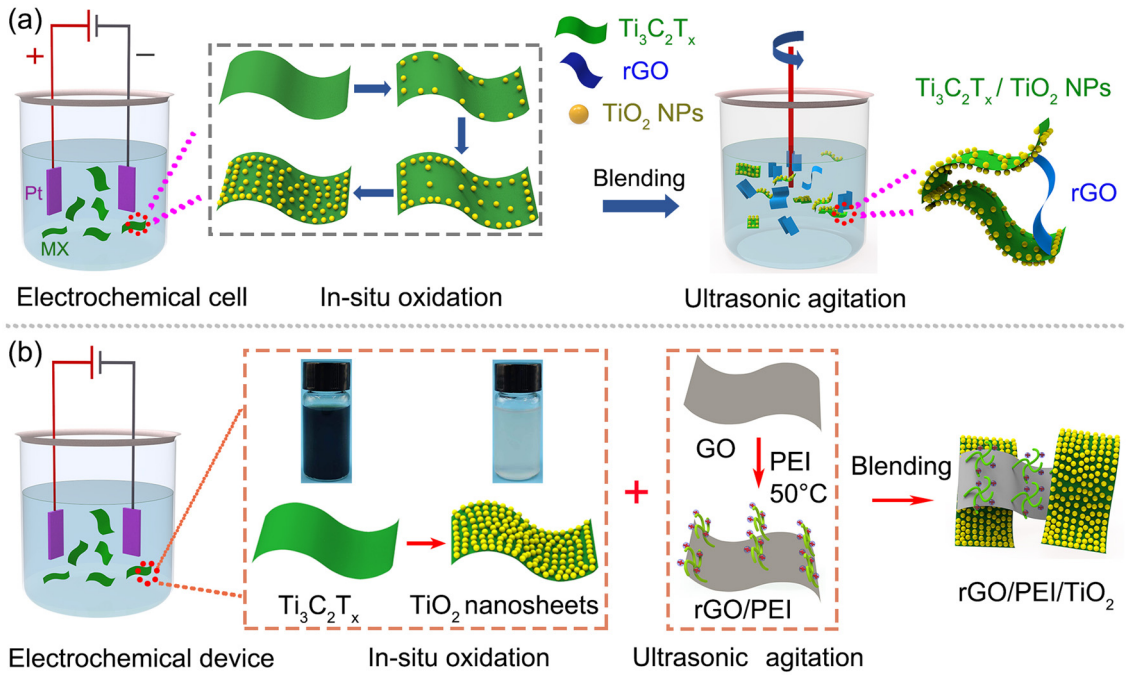

Fig. 8 Solution blending method for preparing graphene-based hybrids as (a) $Ti_3C_2T_x/TiO_2$ NPs/rGO. Reproduced with permission.[105] Copyright from 2024, Wiley-VCH. (b) rGO/PEI/TiO_2. Reproduced with permission.[106] Copyright from 2023, Elsevier.

in situ oxidation of $Ti_3C_2T_x$ NSs and blended them with polyethyleneimine (PEI)-grafted rGO to obtain a rGO/PEI/TiO_2 hybrid, as shown in Fig. 8b. The branched PEI surface is abundant in positively charged amino groups, serving as binding sites to interact with rGO *via* hydrogen bonding or electrostatic attraction. The van der Waals and/or hydrogen bonding are the primary forces responsible for forming the hybrid and constructing the novel electrochemical aptasensing platform. By this fabrication method, various components with specific sensing functions can be easily modified on graphene, exhibiting good voltammetric responses. Despite the simplicity and cost-effectiveness of the solution blending method, it still encounters shortcomings such as weak interactions and the inability to precisely control the structure and layers of the hybrid on substrates. Thus, sensing performance cannot be precisely regulated in an optimum state.

4.2 Interfacial electrostatic self-assembly method

The interfacial electrostatic self-assembly method not only offers high controllability but also provides an inexpensive and straightforward approach to preparing films with diverse graphene-based hybrid structures on substrates. The electrostatic interaction is the primary driving force involved in the interfacial electrostatic self-assembly, through the reaction between graphene and the opposite charged modifiers.[107] Xu *et al.* fabricated the electroactive rGO/SiO_2 nanospheres with huge specific surface area by applying the electrostatic self-assembly method, with Tannic acid (TA) to reduce GO to rGO electrochemically, as illustrated in Fig. 9a.[108,109] The hybrid with a 3D structure, as shown in Fig. 9b, not only prevents the aggregation of rGO but also increases the specific surface area, ultimately improving its sensing performance.

Furthermore, to precisely regulate the film thickness formed on substrates, the layer-by-layer (LBL) assembly method is commonly used to obtain optimal coating films.[112] Multilayered nanostructures composed of graphene and CNTs can be controllably formed on electrodes *via* the LBL method, using electrostatic and π–π interactions, as illustrated in Fig. 9c and d.[110] Typically through the π-stacking interactions, CNTs adhere to GO flakes well and disperse in water stably by the high solubility of GO as a surfactant, facilitating the formation of the films uniformly. The controlled layering process yields optimal performance for sensing applications. The thickness and structure of the LBL-assembled films could be controlled and altered by pH with electrostatic and hydrogen bonding, providing an innovative perspective to fabricate the hybrid film by the LBL method, as shown in Fig. 9e.[111]

In conclusion, an interfacial electrostatic self-assembly offers an optimal method for fabricating a uniform hybrid structure with an enlarged specific surface area and improved target adsorption, thereby boosting its sensing performance.

4.3 *In situ* growth method

The intermolecular interactions between graphene and other specific modifiers can be further enhanced by an *in situ* growth method. The method encompasses two approaches: the *in situ* growth of graphene on a conductive substrate by atomic deposition and the *in situ* growth of modifiers on graphene by solvo-hydrothermal synthesis. Fig. 10a presents the formation process of graphene on the conductive substrate at a

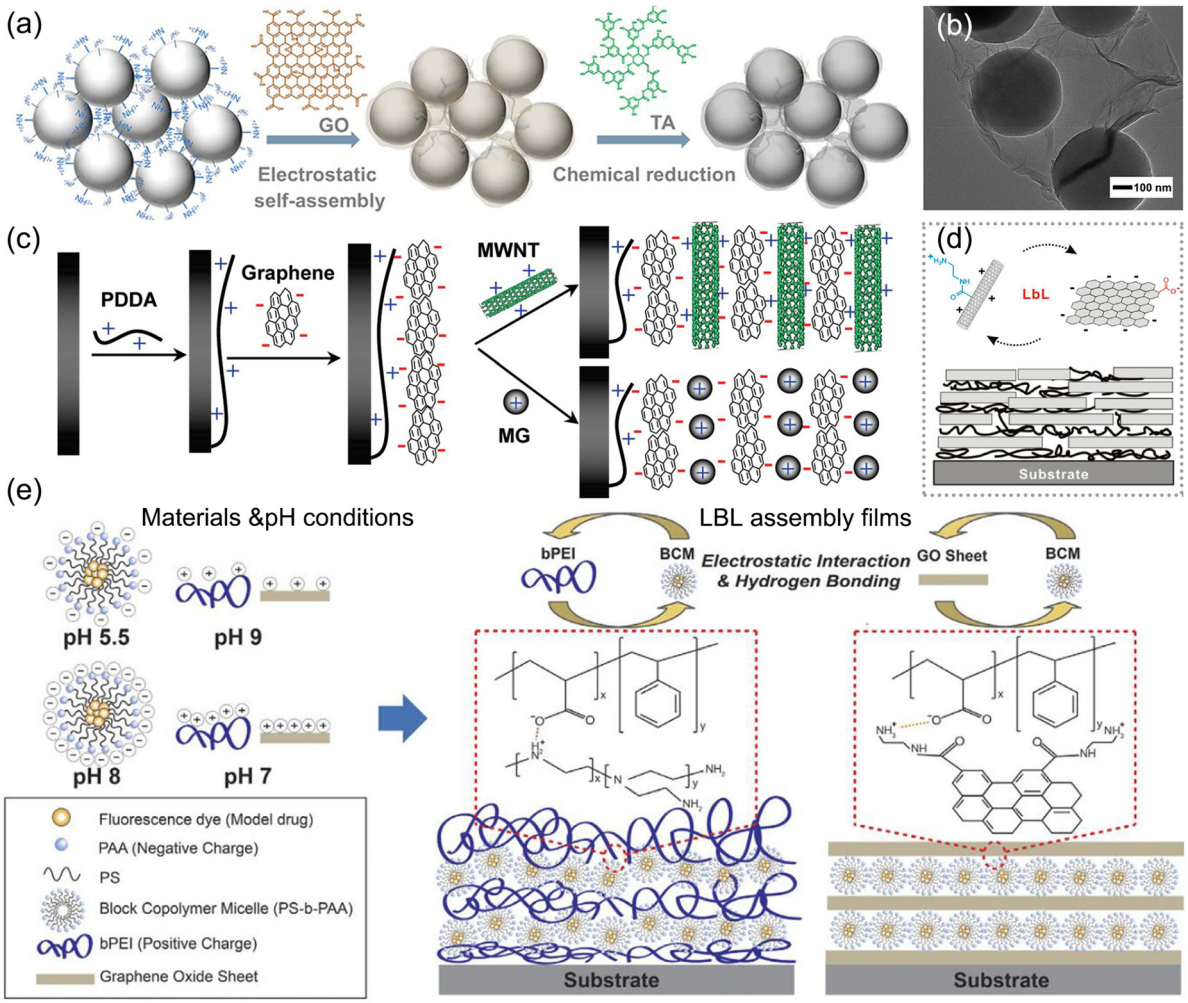

Fig. 9 Interfacial electrostatic self-assembly method for preparing films with various graphene-based hybrid structures. (a) Illustrative preparation of rGO/SiO_2 nanospheres and (b) their TEM image. (a) and (b) Reproduced with permission.[108] Copyright from 2021, American Chemical Society. (c) Controllable formation of electroactive nanostructures by the LBL assembly method. Reproduced with permission.[110] Copyright from 2011, American Chemical Society. (d) Multilayered structure of rGO/CNTs by the LBL assembly method. Reproduced with permission.[109] Copyright from 2010, American Chemical Society. (e) pH regulation on the structure of LBL-assembled multilayered films. Reproduced with permission.[111] Copyright from 2016, Springer Nature.

high temperature in a H_2 atmosphere, providing an effective way to form stable electrodes by achieving strong interfacial contact. Typically, the growth of graphene on high-pressure high-temperature (HPHT) diamond occurs by sp^3-to-sp^2 transformation,[113] as illustrated in Fig. 10b. Fig. 10c and d depict the surface morphology before and after treatment, showcasing the transformation from smooth and flat morphology into an island-like structure. The Raman results presented in Fig. 10e and f reveal the formation of few layers of graphene on HPHT diamond. Fig. 10g presents the mechanism of sp^3-to-sp^2 transformation, showing the precipitation of carbon atoms on molten Cu to form graphene layers at the substrate interface. The transformation results in a strong interfacial bonding between graphene and HPHT, forming stable electrodes of antifouling in practical sensing platforms.

Fig. 10h shows the solvo-hydrothermal method for the *in situ* growth of graphene-based modifiers. Chen *et al.* synthesized a homogeneous nanocomposite of zeolitic imidazole framework-derived Co and nitrogen co-doped carbon polyhedrons and rGO by an *in situ* growth method,[114] as depicted in Fig. 10i. The composite material derived from MOF and rGO demonstrates excellent stability, selectivity and sensitivity towards Metronidazole detection, owing to its enhanced mass transfer, abundant electroactive sites, and superior conductivity. Nehru *et al.* fabricated cobalt-doped Fe_3O_4 nanospheres deposited on GO *via* a facile hydrothermal technique,[66] as shown in Fig. 10j. The schematic Fe_3O_4 crystal structure (site A and B) represents a cubic crystal feature. Here, site A has been occupied by Fe^{3+} and site B has been occupied by an equal number of Fe^{2+} and Fe^{3+} ions. During the introduction of Co^{2+} into the Fe_3O_4 matrix, Fe^{3+} was replaced by Co^{2+} in the site A, while Fe^{2+} was transformed to Fe^{3+} in site-B to sustain electric neutrality. The *in situ* growth of Co-doped Fe_3O_4 on GO improved the performance shortages of the Fe_3O_4 system due to agglomeration and

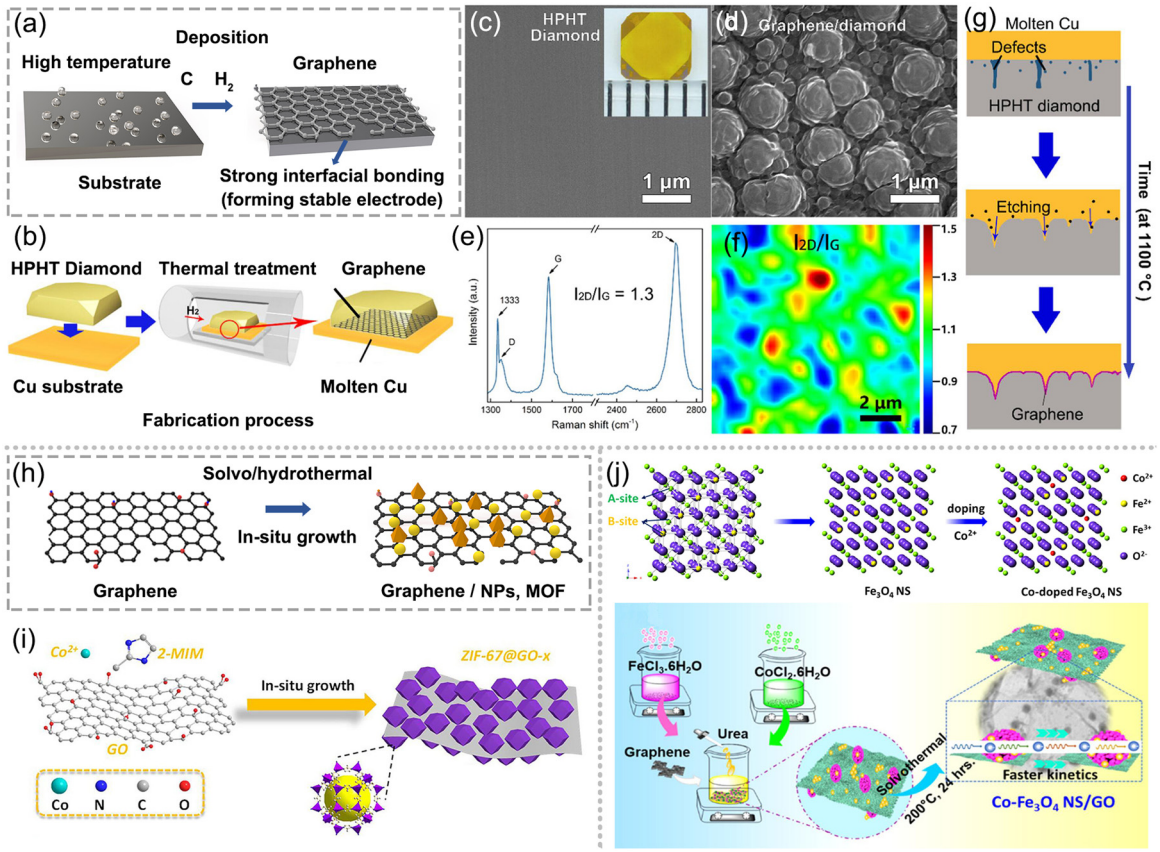

Fig. 10 *In situ* growth method for obtaining strong interfacial contact between graphene and modifiers. (a) Illustration of graphene deposition on the substrate at high temperatures. (b) *In situ* growth of graphene on HPHT diamond by thermal treatment. SEM images of HPHT diamond (c) before and (d) after treatment. (e) Raman spectrum and (f) its mapping of graphene-diamond. (g) Formation mechanism of graphene-diamond. (b)–(g) Reproduced with permission.[113] Copyright from 2018, Elsevier. (h) Solvo-hydrothermal method for the *in situ* growth of graphene-based modifiers. (i) Electrode modified with zeolitic imidazole framework-derived Co and nitrogen co-doped carbon polyhedrons (ZIF-67C) and GO hybrids. Reproduced with permission.[114] Copyright from 2019, Springer. (j) Formation of Co^{2+} doping and synthesis procedure of Co–Fe_3O_4 nanospheres/GO. Reproduced with permission. Copyright from 2021, American Chemical Society.

less conductivity, and enhanced its operation stability due to the strong intermolecular interactions. Thus, the hybrid boosts the electrochemical kinetics and exhibits a low detection limit of 1.04 nM towards chloramphenicol. In summary, the *in situ* growth of graphene-based modifiers renders superior mechanical stability, electrical conductivity, abundant electro-active sites, and electrocatalytic activity and boosts the electron-transfer kinetics for antibiotic detection.[40,60,115]

5. Portable electrochemical platform for the on-site monitoring of antibiotics in real samples

Conventional electrodes and electrochemical apparatus based on the tag/anti-tag system are bulky and time/energy consuming, hindering their potential for the on-site monitoring of environmental, clinical and food samples. Thus, the fabrication of miniaturized electrochemical platforms has attracted attention.[116–118] Integrating miniaturized electrodes as screen printed, flexible forms, microfluidic systems and potentiostat into a portable detection platform with automation will facilitate its on-site applications, exhibiting superiorities as portability, cost-efficiency, data availability in less time and manipulation outside the laboratories with facility.[119–122] In this section, the state-of-the-art portable electrochemical platform can be summarized into three categories: (a) glove-based wearable sensors for monitoring antibiotics in food samples, (b) epidermal and microneedle-based wearable device for clinical monitoring, and (c) microfluidic electrochemical chip proposed for multianalyte monitoring.

5.1 Glove-based wearable sensors for monitoring antibiotics in food samples

When considering antibiotic monitoring in the food industry, the needs for real-time, high-accuracy and on-site analysis are imperative for ensuring the food safety and preservation. Glove-based wearable sensors were developed for electrochemical monitoring antibiotics in food samples,[77,123] as depicted in Fig. 11a. Mishra *et al.* reported a glove-based wearable sensor with a printable electrode system to monitor pesticide-contaminated agricultural products.[123,124] Before

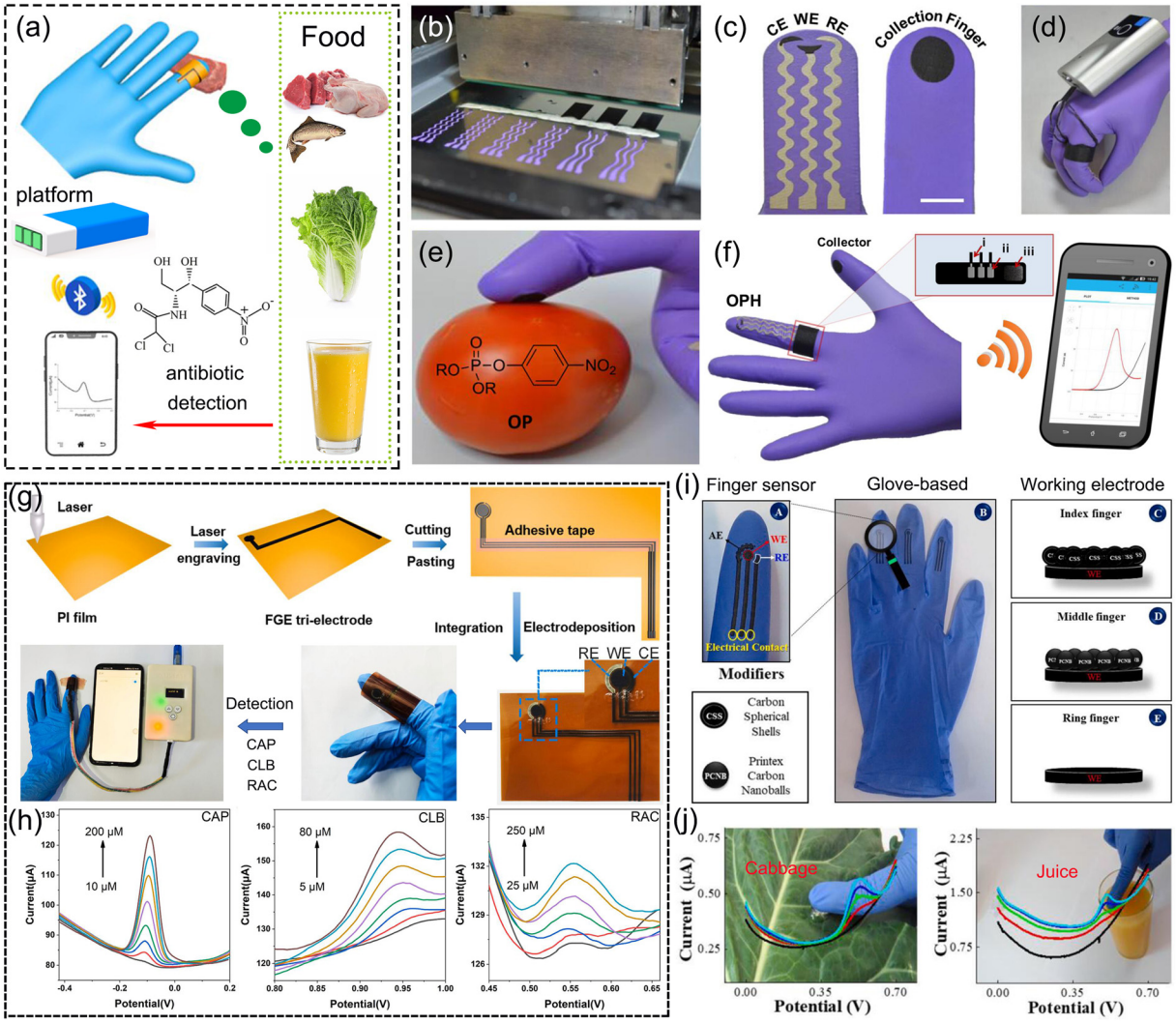

Fig. 11 Glove-based wearable sensors for antibiotic detection. (a) Schematic. (b) Configuration of the glove-based stretchable device, with (c) scan finger (left) containing biosensing electrodes and collection finger (right). (d) Photograph of the glove-based sensor, containing a ring bandage connecting the electrodes with a portable potentiostat. (e) and (f) Swipe sampling protocol on the glove to complete the sensing function. (b)–(f) Reproduced with permission.[123] Copyright from 2017, American Chemical Society. (g) A laser-induced flexible electrochemical sensing system integrated on the finger. (h) DPV curves of antibiotic detection on flexible graphene electrodes. (g) and (h) Reproduced with permission.[77] Copyright from 2022, Elsevier. (i) and (j) Photograph of the glove-based sensor for on-site monitoring in food samples. Reproduced with permission.[124] Copyright from 2021, Elsevier.

electrochemical measurements, swipe sampling with finger scan on agricultural products was carried out for collecting analyte residues. The electrochemical cell was formed by joining the scan finger and collection finger to perform measurements. Portable potentiostat was loaded along with electrodes to emit signals through wireless transmission to a smartphone. The fabrication and sensing process of glove-based sensors are exhibited in Fig. 11b–f. The proposed wearable "lab-on-a-glove" platform exhibits potential for future monitoring antibiotics in food supervision.

Li *et al.* constructed a laser-induced flexible electrochemical sensing system on fingers for rapid real-time on-site identification of chloramphenicol, clenbuterol, and ractopamine in meat.[77] As depicted in Fig. 11g, flexible graphene electrodes were facilely patterned and prepared by CO_2 laser and integrated with disposable blue nitrile gloves for constructing a finger-based sensing system. Through the connection with a portable electrochemical analyser, electrochemical signals could be received by the directly touching object under DPV tests with fingertips and displayed on mobile phone. The LOD of chloramphenicol and the other two feed additives, namely, clenbuterol and ractopamine was 2.70, 1.29 and 7.81 μM, respectively, enabling the successful application of the sensing platform on the finger for food security, as shown in Fig. 11h. Raymundo-Pereira *et al.* developed a non-enzymatic sensor system printed on three fingers of a rubber glove for the detection of carbendazim in food samples, as depicted in Fig. 11i.[124] In Fig. 11j, the sensor was capable of monitoring

carbendazim in a rapid and cost-effective manner by directly touching the samples with the glove, exhibiting 47 nM LOD for carbendazim by the DPV method, and was successfully applied for cabbage and juice samples.

5.2 Epidermal and microneedle-based wearable device for clinical monitoring

In clinical medicine critically ill patients are treated with inadequate antibiotic dosing, resulting in antimicrobial resistance or bad antimicrobial therapy for infections.[125] The wide ranging variations in individual pharmacokinetic–pharmacodynamic target attainment request the emergency for accurate antibiotic monitoring to facilitate individualized dose optimization.[125] Thus, the promotion of wearable biosensor is necessary for the on-site and non-invasive monitoring of antibiotics in human interstitial fluids such as sweat to diagnose disease at early stage, leading to the development of epidermal and microneedle-based wearable sensors for antibiotic monitoring in clinical treatment. As an invasive biofluid with abundant physiological information, sweat is suitably used to be a target fluid for health monitoring combined with an epidermal sensor. Fig. 12a depicts the epidermal sensor involving the integration of skin multilayer models. Tai *et al.* fabricated a wearable sweat band (s-band) platform for on-body and non-invasive drug monitoring, as presented in Fig. 12b–d.[126] Printed circuit boards and carbon electrodes were integrated into this wearable platform to construct the flexible electrochemical sensor, and DPV measurement was employed for caffeine detection after sweat extraction by the iontophoresis method. This s-band portable platform may achieve continuous and non-invasive recognition of antibiotic levels, showing the potential for future applications in clinical medicine and healthcare-related system.

To overcome the difficulty of accessing human interstitial fluids, the microneedle array has been developed to substitute hypodermic needles for transdermal drug delivery and sampling human interstitial fluids. Microneedle-based wearable sensors are constructed by the integration of multiple microneedle electrodes on a wearable patch device for real-time diagnostic evaluation of the antibiotic level.[75,127] Fig. 12e illustrates the microneedle transdermal sensing *via* interstitial fluid access. Rawson *et al.* developed a microneedle β-lactamase biosensor for real-time and minimally invasive monitoring of penicillin V *in vivo*, as shown in Fig. 12f and g.[75] The open

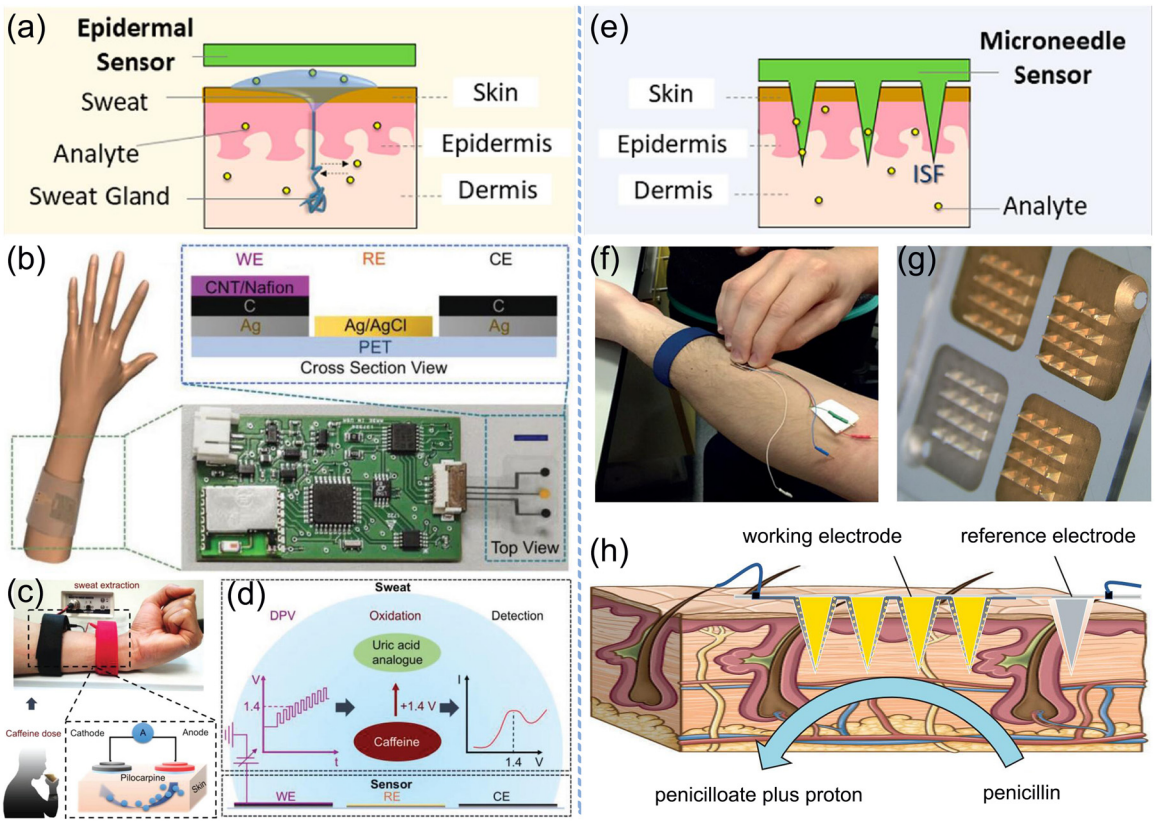

Fig. 12 Epidermal and microneedle-based wearable sensors through sweat or interstitial fluid sampling for antibiotic detection in clinical treatment. (a) Scheme of an epidermal sensor involving the integration of skin multilayer models. Reproduced with permission.[116] Copyright from 2020, American Chemical Society. (b) A wearable platform integrated into a wristband for noninvasive drug monitoring and the cross-section view of the flexible electrodes. (c) Sweat extraction through iontophoresis method and (d) DPV signals from caffeine detection. (b)–(d) Reproduced with permission.[126] Copyright from 2018, Wiley-VCH. (e) Scheme of microneedle transdermal sensing *via* interstitial fluid access. (f) and (g) Microneedle array biosensor to the forearm with 60 s firm pressure. (h) Diagram of the penetration of microneedle array into the dermal-interstitial space. (f)–(h) Reproduced with permission.[75] Copyright from 2019, Elsevier.

circuit potential of the working electrode *versus* the reference electrode was recorded as detection signals, as depicted in Fig. 12h. Penicillin V, as a common antibiotic to cure bacterial infections, diffuses from the extracellular fluid to the hydrogel layer, and hydrolysed to penicilloate and a proton by β-lactamase. Therefore, the increasing concentration of penicillin V in the tissue promoted the protons generated at the sensor surface, inducing the elevations of open circuit potential. The LOD of penicillin V by the microneedle method was estimated as 0.17 mg L^{-1}, prospecting potential antibiotic monitoring for individualized dose optimization.

5.3 Microfluidic electrochemical chip proposed for multianalyte monitoring

Point-of-care (POC) monitoring proposes the requirements for rapid, accurate, and low sample volume detection in a regulated bioanalytical environment. Moreover, simultaneous detection of multi-antibiotics in human biofluids with a very low volume raises the need of a multiplexed biosensor platform. Here, a microfluidic electrochemical chip provides the opportunity to achieve multi-antibiotic POC monitoring with operation simplicity and size miniaturization.[74,128,129]

Kling *et al.* constructed a microfluidic platform enabling the electrochemical readout of up to eight enzyme-linked assays for the simultaneous detection of two antibiotics, namely, tetracycline and streptogramin in spiked human plasma, as presented in Fig. 13a.[74] The microchannel network contained a single electrochemical cell with a three-electrode setup for the amperometric signal detection, and was connected to the substrate solution reservoir *via* the common to the outlet. The signal amplification of antibiotic detection was obtained using a defined stop-flow measurement technique, and the corresponding function principle is illustrated in Fig. 13b. The bound enzyme glucose oxidase generated limited H_2O_2 when the glucose substrate was constantly supplied in the microchannel and catalyzed the reaction to more H_2O_2 when the flow was stopped. When restarting the flow, the accumulated clouds were flushed over the working electrode, and the generated peak signal from H_2O_2 oxidation was measured amperometrically, as depicted in Fig. 13c and d. The formula of antibiotic detection in the human plasma involved a DNA–protein

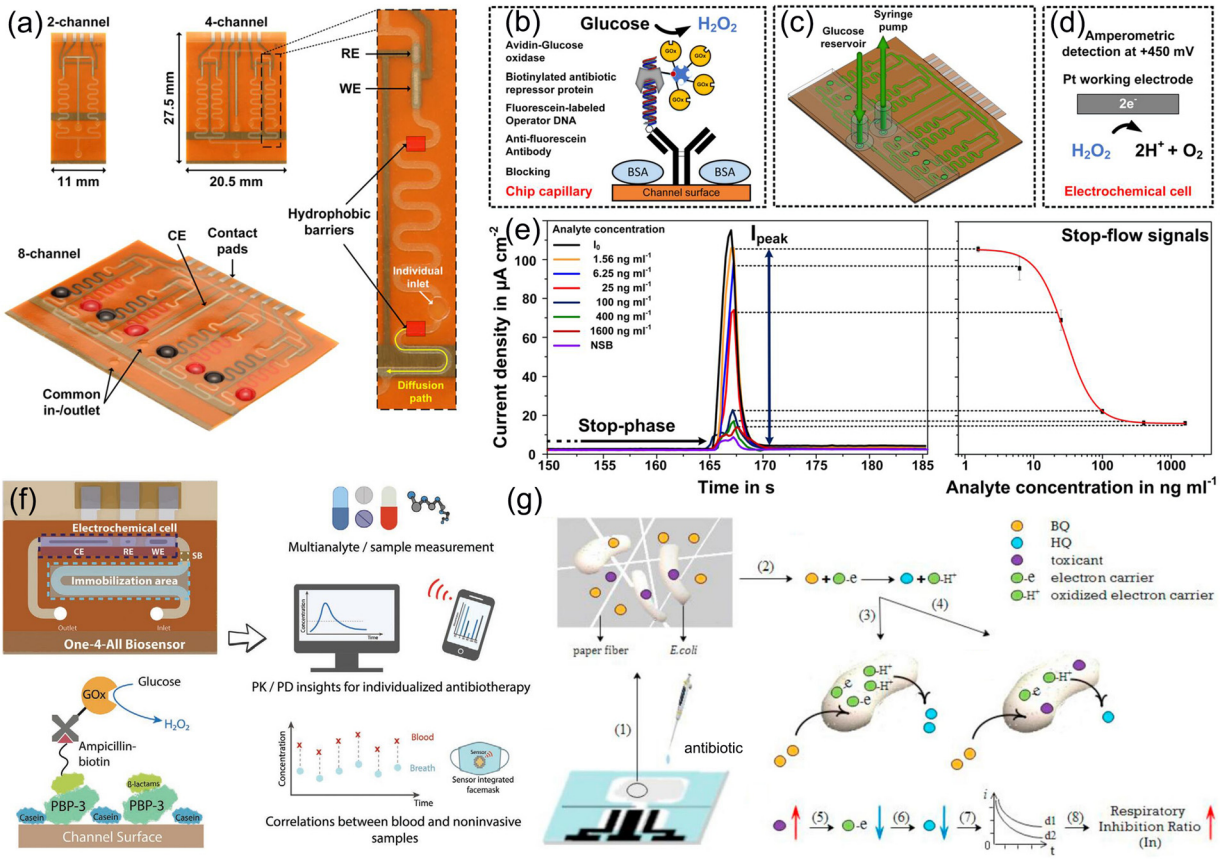

Fig. 13 Microfluidic electrochemical chip proposed for the simultaneous detection of multi-antibiotics. Microfluidic biosensors comprising multiple immobilization sections: (a) system configuration; (b) measurement principle; (c) sensing device; (d) reaction mechanism of H_2O_2 oxidation at the working electrode; (e) amperometric responses and the resulting on-chip calibration curve. (a)–(e) Reproduced with permission.[74] Copyright from 2016, American Chemical Society. (f) A microfluidic electrochemical biosensor constructed for multianalyte monitoring based on enzymatic catalysis. Reproduced with permission.[128] Copyright from 2022, Wiley-VCH. (g) Paper-based microfluidic device for multianalyte monitoring based on the respiratory inhibition of *E. coli*. Reproduced with permission.[129] Copyright from 2019, Elsevier.

interaction sensing mechanism.[74] The repressor protein showed a conformational change in the antibiotic presence, indicating no binding capability to their designated operator DNA. The higher concentration of antibiotics resulted in lesser proteins bound to operator DNA, demonstrating the decreased electrochemical signal. The platform concluded the LOD of 6.33 and 9.22 ng mL^{-1} for tetracycline and pristinamycin respectively, as shown in Fig. 13e.

Dincer *et al.* constructed a microfluidic electrochemical biosensor consisting of an electrochemical cell, immobilized region, and a hydrophobic barrier in prevention of electrode fouling during detection, as depicted in Fig. 13f.[128] The measurement signal could be obtained from the catalysis reaction of H_2O_2 by glucose oxidase, and the platform proved the feasibility for the on-site monitoring of multi-antibiotics such as piperacillin, tazobactam and meropenem in human biofluids. Zhang *et al.* developed a paper-based microfluidic device for multianalyte monitoring, as displayed in Fig. 13g,[129] which was operated based on the respiratory inhibition of *E. coli* due to the interference of antibiotics in the environment, resulting in the amplification of electrochemical signal. The paper-based microfluidic platform offers a new perspective for the on-site monitoring of multi-antibiotics.

In summary, a portable electrochemical platform for the on-site monitoring of antibiotics depends on specific application requirements, leading to varying applicability of the three wearable scenarios. For the convenient monitoring of antibiotics in food samples, a wearable ''lab-on-a-glove'' platform shows great potential to achieve the goal. Yet, this platform still faces a bottleneck in the limit of detection of antibiotics.

For the non-invasive monitoring of antibiotics in human interstitial fluids such as sweat and blood, an epidermal and microneedle-based platform is the optimum choice for clinical monitoring. It can achieve trace-level or ultra trace-level detection limits of target antibiotics.

Moreover, the microfluidic electrochemical chip provides an opportunity for the simultaneous detection of multi-antibiotics in human biofluids with accuracy, but it suffers from the limitation of complicated device construction. The selection of graphene-based electrodes for diverse wearable platforms is contingent upon specific application scenarios, whereas graphene facilitates signal amplification during detection periods.

6. Conclusions and future perspectives

The excessive emissions of residual antibiotics pose an increasing threat to the ecosystem and human health due to extensive unreasonable use of antibiotics to cure various infectious diseases in livestock and humans. For human health and ecological safety, it is critical to determine the residual antibiotics with accuracy and convenience. In this regard, electrochemical detection platforms for antibiotics have been developed due to their high sensitivity, simplicity, and time saving. This comprehensive review retrospects the recent

Table 2 Graphene-based electrochemical sensors for antibiotic detection

Graphene-based modifying electrode		Analyte	Technique	Detection range	LOD	Real sample	Ref.
Noble metal NPs	rGO/Ag NPs/NiF	Amikacin	DPV	0.05–15.0 μM	38.0 nM	Urine	131
	rGO/Au NPs/Pd NPs	Lomefloxacin Amoxicillin	SWV	4.0–500.0 μM, 30.0–350.0 μM	38.0 nM 9.0 μM	Urine	56
	rGO/Au NPs	Chloramphenicol	LSV	2.0–80.0 μM	0.59 μM	Eye drops	53
	rGO/Pd NPs	Chloramphenicol	DPV	0.05–1.0 μM	0.05 μM	Honey, tap water	132
	GO/Au NPs	Clindamycin	SWV	0.95–140.0 μM	0.29 μM	Urine, river water	73
	rGO/Au NPs/polypyrrole	Doxorubicin	CV	0.02 μM–25.0 mM	0.02 μM	Drugs	133
	rGO/Cu NPs	Metronidazole	*i*–t	0.002–210.0 μM	0.6 nM	Drugs	60
	GO/Ag NPs	Metronidazole	*i*–*t*	0.09–4594.0 μM	0.07 μM	Drugs	134
CNTs	GO/CNTs	Azithromycin	LSV	0.1–10 μM	0.07 μM	Urine, capsules	44
	rGO/VS_2/CNTs	Azithromycin	DPV	2.8–300 nM	0.9 nM	Human serum, urine	67
	rGO/CNTs	Natamycin	ASV	0.05–2.5 μM	0.01 μM	Red wine, beverage	58
	GO-CNTs	Tetracycline	DPV	20.0–310.0 μM	0.36 μM	River water	54
MOF	rGO/Z-800	Chloramphenicol	DPV	1.0–180.0 μM	0.25 μM	Milk, honey	135
	rGO/NH_2-UiO-66	Ciprofloxacin	ASV	0.02–1.0 μM	6.67 nM	Tap water, lake water	62
Metal oxides	rGO/Eu_2O_3	Chloramphenicol	*i*–*t*	0.02–800.3 μM	1.32 nM	Milk, honey	63
	rGO/TiO_2	Furazolidone	DPV	1.0–150.0 pM	0.43 pM	Blood serum	136
	Graphene/$MnMoO_4$	Ornidazole	*i*–*t*	0.01–0.77 μM	0.85 nM	River water	68
	Graphene/ZnO	Sulfamethoxazole Trimethoprim	DPV	1–170 μM 1–170 μM	0.4 μM 0.3 μM	Urine, serum, lake water	42
	GO/Fe_3O_4/Co	Chloramphenicol	DPV	0.005–152.2 μM	1.04 nM	Food	66
Immunosensors	Graphene/prussian/chitosan	Kanamycin	DPV	0.04–28.8 nM	13.0 pM	Food	137
	GO/P(NIPAm-MPTC-GMA)	Streptomycin	DPV	0.09–170.0 nM	2.89 pM	Milk	38
	Graphene/Zn/Ni-ZIF/Au NPs	Monensin	DPV	0.38–150.0 nM	0.17 nM	Milk	138
	rGO/Au NPs/peroxidase	Oxytetracycline	DPV	1.0 pM–4.0 μM	1.0 pM	Food	41
Aptamers	GO/Ag NPs/aptamer	Chloramphenicol	DPV	10.0 pM–0.2 μM	3.3 pM	Milk, honey	65
	rGO/Au NPs/aptamer	Ciprofloxacin	SWV	0.001–1.0 μM	1.0 nM	Milk	46
	Graphene/Pt–Cu alloy/aptamer	Kanamycin	DPV	1.0 pM–10.3 nM	0.87 pM	Food	39
	GO/aptamer	Tetracycline	EIS	0.1 pM–10.0 μM	0.03 pM	Blood serum	139
	GR/Fe_3O_4/Au NPs/aptamer	Streptomycin	DPV	0.09–340.0 nM	0.05 nM	Milk	57

advances in graphene-based electrochemical sensors for antibiotics, focusing on the theoretical description of electrochemical sensing mechanisms and practical applications of portable electrochemical platforms for on-site monitoring. Table 2 summarizes the sensor performance, including the detection linear range and LOD. Obviously, graphene-based sensors including immunosensors and aptasensors demonstrate superior detection performance with an LOD several thousands of times lower than that of sensors modified with noble metal NPs, CNTs, metal oxides and MOFs. This superiority is attributed to the specific antigen–antibody reaction and the precise recognition and binding with the target antibiotic.[31] Additionally, modifiers such as noble metal NPs, CNTs, metal oxides and MOFs have been extensively applied to sensing electrodes due to their excellent biocompatibility, large surface area, high electron transfer rate, good chemical stability and mechanical strength.[50,62,67,130]

Although electrochemical sensing methodology has been successfully applied for antibiotic detection, there are still many scientific and technical challenges that need to be overcome in the future. As illustrated in Fig. 14, the current challenges can be listed as follows:

(1) The category distribution of electrochemical sensors for antibiotics is inhomogeneous. Due to the presence of multiple antibiotics in the environment, the current sensors primarily designed for common antibiotics, typically amphenicols and aminoglycosides, are not sufficient and beneficial for the trace determination of antibiotic residues in the environment. Constructing electrochemical sensors for antibiotics covering as many species as possible is necessary.

(2) The electrodes designed on graphene-based modifiers without the selective capability suffer technical difficulty in the selectivity of target antibiotics, especially in the presence of multiple antibiotic species with similar structures in real samples. While for the current immunosensors or aptasensors aimed to the selectivity issue, the enduring preservation and maintenance of bioactive molecules as immune components and aptamers pose a challenge to ensure their consistence performance over time. Thus, constructing electrochemical sensors for antibiotics that possess both high sensitivity and excellent selectivity towards various types of antibiotics is still urgent and meaningful. Particularly, ensuring the long-term stability of graphene-based sensors is essential for the sustained monitoring and practical applications.

(3) The theoretical interpretation of the antibiotic sensing mechanism is vitally important for pursuing excellent detection performance with various electrochemical techniques. Yet, the sensing mechanism of antibiotics reported in current research papers mainly refers to the analysis of electrical responses. The redox reaction process involving electron

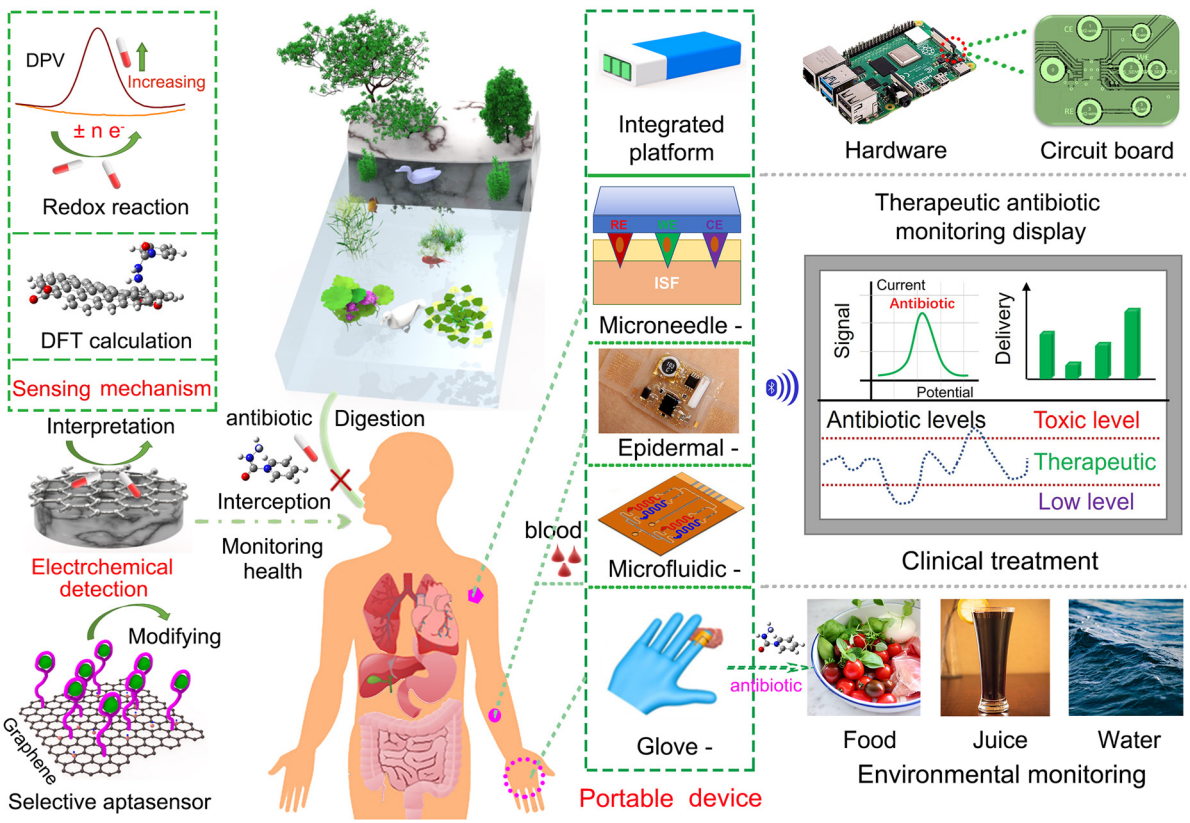

Fig. 14 Future perspectives of graphene-based electrochemical sensors for antibiotics. The successful construction of objective sensors needs to focus on the theoretical description of electrochemical sensing mechanisms and practical applications for the on-site monitoring of antibiotics in the fields of healthcare monitoring, environmental protection, and food safety.

transfer and interfacial interactions between the electrode surface and the adsorbed molecules at the atomic level should be carried out for in-depth exploration, using theoretical calculation software of the quantum-mechanical method. It not only aggravates the interpretation of the antibiotic sensing mechanism theoretically, but also provides key information about the specific nanomaterials with sensitivity to every antibiotic.

(4) Various forms of antibiotics exist in environment such as in river water, food, human serum, urine, and honey, increasing the difficulty for the development of portable electrochemical platforms for the on-site monitoring of antibiotics. Thus, the platform should be automated, conforming to the scenario requirements of antibiotic detection in various real samples. The optimization of the microneedle, epidermal or microfluidic platform is hopeful for on-site therapeutic antibiotic monitoring in human biofluids towards clinical treatment. Glove-based wearable sensors show potential for the future on-site monitoring of antibiotics in the environment. Moreover, the cost of constructing graphene-based electrochemical sensors to achieve mass production should be reduced to an accepted extent to realize the commercial application.

Overall, the future development of graphene-based electrochemical sensors for antibiotics requires addressing the challenges at the technological, engineering, and application levels. The deep exploration within the scope enables the further utilization of the sensors in the fields of healthcare monitoring, environmental protection, and food safety.

Data availability

The raw/processed data required to reproduce the findings of this study cannot be shared at this time due to legal/ethical reasons.

Conflicts of interest

The authors declare no conflict of interest.

Acknowledgements

C. T. Lin acknowledges the financial support by the National Natural Science Foundation of China (52272053), the National Key R&D Program of China (2022YFA1203100), and Ningbo Key Scientific and Technological Project (2021Z120, 2021Z115, 2022Z084).

References

1 K. K. Brandt, A. Amezquita, T. Backhaus, A. Boxall, A. Coors, T. Heberer, J. R. Lawrence, J. Lazorchak, J. Schonfeld, J. R. Snape, Y. G. Zhu and E. Topp, *Environ. Int.*, 2015, **85**, 189–205.
2 H. K. Allen, J. Donato, H. H. Wang, K. A. Cloud-Hansen, J. Davies and J. Handelsman, *Nat. Rev. Microbiol.*, 2010, **8**, 251–259.
3 R. F. Yuan, Y. D. Zhu, B. H. Zhou and J. Y. Hu, *Chem. Eng. J.*, 2019, **359**, 1527–1536.
4 B. J. A. Berendsen, J. Lahr, C. Nibbeling, L. J. M. Jansen, I. E. A. Bongers, E. L. Wipfler and M. G. M. van de Schans, *Chemosphere*, 2018, **204**, 267–276.
5 Y. Luo, D. Mao, M. Rysz, Q. Zhou, H. Zhang, L. Xu and P. J. J. Alvarez, *Environ. Sci. Technol.*, 2010, **44**, 7220–7225.
6 D. Tadic, M. J. Bleda Hernandez, F. Cerqueira, V. Matamoros, B. Pina and J. M. Bayona, *J. Hazard. Mater.*, 2021, **401**, 123424.
7 J. C. Underwood, R. W. Harvey, D. W. Metge, D. A. Repert, L. K. Baumgartner, R. L. Smith, T. M. Roane and L. B. Barber, *Environ. Sci. Technol.*, 2011, **45**, 3096–3101.
8 R. Singh, A. P. Singh, S. Kumar, B. S. Giri and K.-H. Kim, *J. Cleaner Prod.*, 2019, **234**, 1484–1505.
9 M. Kumar, S. Jaiswal, K. K. Sodhi, P. Shree, D. K. Singh, P. K. Agrawal and P. Shukla, *Environ. Int.*, 2019, **124**, 448–461.
10 K. Kummerer, *Chemosphere*, 2009, **75**, 417–434.
11 K. Kummerer, *Chemosphere*, 2009, **75**, 435–441.
12 H. Y. Shen and H. L. Jiang, *Anal. Chim. Acta*, 2005, **535**, 33–41.
13 H. Y. Liu, S. L. Lin and M. R. Fuh, *Talanta*, 2016, **150**, 233–239.
14 A. Azzouz and E. Ballesteros, *Food Chem.*, 2015, **178**, 63–69.
15 J. N. Baby, B. Sriram, S. F. Wang and M. George, *J. Hazard. Mater.*, 2021, **408**, 124940.
16 T. Kokulnathan, T. J. Wang, N. Duraisamy, E. A. Kumar and S. An Ni, *J. Hazard. Mater.*, 2021, **412**, 125257.
17 T. Kokulnathan and S. M. Chen, *J. Hazard. Mater.*, 2020, **384**, 121304.
18 F. Chen, Z. Fan, Y. Zhu, H. Sun, J. Yu, N. Jiang, S. Zhao, G. Lai, A. Yu, C. T. Lin, C. Ye and L. Fu, *Materials*, 2020, **13**, 777.
19 N. A. Shad, S. Z. Bajwa, N. Amin, A. Taj, S. Hameed, Y. Khan, Z. Dai, C. Cao and W. S. Khan, *J. Hazard. Mater.*, 2019, **367**, 205–214.
20 Y. Zhang, Z. Liu, Y. Wang, X. Kuang, H. Ma and Q. Wei, *J. Hazard. Mater.*, 2020, **398**, 122778.
21 M. Li, T. Zhe, F. Li, R. Li, F. Bai, P. Jia, T. Bu, Z. Xu and L. Wang, *J. Hazard. Mater.*, 2022, **435**, 129059.
22 W. Dai, L. Lv, J. Lu, H. Hou, Q. Yan, F. E. Alam, Y. Li, X. Zeng, J. Yu, Q. Wei, X. Xu, J. Wu, N. Jiang, S. Du, R. Sun, J. Xu, C. P. Wong and C. T. Lin, *ACS Nano*, 2019, **13**, 1547–1554.
23 Y. Zhu, Q. Tian, X. Li, L. Wu, A. Yu, G. Lai, L. Fu, Q. Wei, D. Dai, N. Jiang, H. Li, C. Ye and C. T. Lin, *Biosensors*, 2021, **11**, 462.
24 N. Cui, P. Guo, Q. Yuan, C. Ye, M. Yang, M. Yang, K. W. A. Chee, F. Wang, L. Fu, Q. Wei, C. T. Lin and J. Gao, *Sensors*, 2019, **19**, 2979.
25 A. Criado, M. Melchionna, S. Marchesan and M. Prato, *Angew. Chem., Int. Ed.*, 2015, **54**, 10734–10750.
26 Y. Yao, C. Jiang and J. Ping, *Biosens. Bioelectron.*, 2019, **123**, 178–184.
27 S. Liu, G. Lai, H. Zhang and A. Yu, *Microchim. Acta*, 2017, **184**, 1445–1451.

28 O. Bunkoed, P. Raksawong, R. Chaowana and P. Nurerk, *Talanta*, 2020, **218**, 121168.
29 Q. Wang, Q. Xue, T. Chen, J. Li, Y. Liu, X. Shan, F. Liu and J. Jia, *Chin. Chem. Lett.*, 2021, **32**, 609–619.
30 L. Fu, S. Mao, F. Chen, S. Zhao, W. Su, G. Lai, A. Yu and C. T. Lin, *Chemosphere*, 2022, **297**, 134127.
31 A. Joshi and K. H. Kim, *Biosens. Bioelectron.*, 2020, **153**, 112046.
32 L. Lan, Y. Yao, J. Ping and Y. Ying, *Biosens. Bioelectron.*, 2017, **91**, 504–514.
33 L. Qian, S. Durairaj, S. Prins and A. Chen, *Biosens. Bioelectron.*, 2021, **175**, 112836.
34 T. T. T. Tran, M. N. Do, T. N. H. Dang, Q. H. Tran, V. T. Le, A. Q. Dao and Y. Vasseghian, *Environ. Res.*, 2022, **208**, 112744.
35 T. W. Chen, U. Rajaji, S. M. Chen, S. Chinnapaiyan and R. J. Ramalingam, *Ultrason. Sonochem.*, 2019, **56**, 430–436.
36 Z. Jiang, G. Li and M. Zhang, *Sens. Actuators, B*, 2016, **228**, 59–65.
37 M. Rouhani and A. Soleymanpour, *Microchem. J.*, 2021, **165**, 106160.
38 X. He, H. Han, L. Liu, W. Shi, X. Lu, J. Dong, W. Yang and X. Lu, *ACS Appl. Mater. Interfaces*, 2019, **11**, 13676–13684.
39 X. Qin, Y. Yin, H. Yu, W. Guo and M. Pei, *Biosens. Bioelectron.*, 2016, **77**, 752–758.
40 X. Zhan, G. Hu, T. Wagberg, S. Zhan, H. Xu and P. Zhou, *Microchim. Acta*, 2015, **183**, 723–729.
41 S. Liu, Y. Wang, W. Xu, X. Leng, H. Wang, Y. Guo and J. Huang, *Biosens. Bioelectron.*, 2017, **88**, 181–187.
42 X. Yue, Z. Li and S. Zhao, *Microchem. J.*, 2020, **159**, 105440.
43 Y. Sun, J. He, G. I. N. Waterhouse, L. Xu, H. Zhang, X. Qiao and Z. Xu, *Sens. Actuators, B*, 2019, **300**, 126993.
44 K. Zhang, L. Lu, Y. Wen, J. Xu, X. Duan, L. Zhang, D. Hu and T. Nie, *Anal. Chim. Acta*, 2013, **787**, 50–56.
45 W. Lian, S. Liu, J. Yu, X. Xing, J. Li, M. Cui and J. Huang, *Biosens. Bioelectron.*, 2012, **38**, 163–169.
46 M. Mahmoudpour, H. Kholafazad-Kordasht, J. E. Nazhad Dolatabadi, M. Hasanzadeh, A. H. Rad and M. Torbati, *Anal. Chim. Acta*, 2021, **1174**, 338736.
47 A. Wong, T. A. Silva, F. C. Vicentini and O. Fatibello-Filho, *Talanta*, 2016, **161**, 333–341.
48 S. Li, X. Ma, C. Pang, H. Li, C. Liu, Z. Xu, J. Luo and Y. Yang, *Anal. Chim. Acta*, 2020, **1127**, 69–78.
49 W. Guo, A. Umar, M. A. Alsaiari, L. Wang and M. Pei, *Microchem. J.*, 2020, **158**, 105270.
50 M. Yadav, V. Ganesan, R. Gupta, D. K. Yadav and P. K. Sonkar, *Microchem. J.*, 2019, **146**, 881–887.
51 V. Mariyappan, M. Keerthi, S. M. Chen and T. Jeyapragasam, *J. Colloid Interface Sci.*, 2021, **600**, 537–549.
52 K. D. Ramadhass, M. Ganesan, T.-W. Chen, S.-M. Chen, Q. Hao, W. Lei and G. Gopalakrishnan, *Colloids Surf., A*, 2021, **628**, 127275.
53 J. Borowiec, R. Wang, L. Zhu and J. Zhang, *Electrochim. Acta*, 2013, **99**, 138–144.
54 A. Wong, M. Scontri, E. M. Materon, M. R. V. Lanza and M. D. P. T. Sotomayor, *Electroanal. Chem.*, 2015, **757**, 250–257.
55 R. Karthik, M. Govindasamy, S.-M. Chen, V. Mani, B.-S. Lou, R. Devasenathipathy, Y.-S. Hou and A. Elangovan, *J. Colloid Interface Sci.*, 2016, **475**, 46–56.
56 N. Kumar, Rosy and R. N. Goyal, *Sens. Actuators, B*, 2017, **243**, 658–668.
57 J. Yin, W. Guo, X. Qin, J. Zhao, M. Pei and F. Ding, *Sens. Actuators, B*, 2017, **241**, 151–159.
58 X. Yang, X. Yu, Y. Heng and F. Wang, *Electroanal. Chem.*, 2018, **816**, 54–61.
59 T. Kokulnathan, T. S. K. Sharma, S.-M. Chen, T.-W. Chen and B. Dinesh, *J. Taiwan Inst. Chem. Eng.*, 2018, **89**, 26–38.
60 V. Velusamy, S. Palanisamy, T. Kokulnathan, S. W. Chen, T. C. K. Yang, C. E. Banks and S. K. Pramanik, *J. Colloid Interface Sci.*, 2018, **530**, 37–45.
61 M. Govindasamy, S. F. Wang, S. Kumaravel, R. J. Ramalingam and H. A. Al-Lohedan, *Ultrason. Sonochem.*, 2019, **52**, 382–390.
62 X. Fang, X. Chen, Y. Liu, Q. Li, Z. Zeng, T. Maiyalagan and S. Mao, *ACS Appl. Nano Mater.*, 2019, **2**, 2367–2376.
63 U. Rajaji, S. Manavalan, S.-M. Chen, M. Govindasamy, T.-W. Chen and T. Maiyalagan, *Composites, Part B*, 2019, **161**, 29–36.
64 M. H. Ghanbari, A. Khoshroo, H. Sobati, M. R. Ganjali, M. Rahimi-Nasrabadi and F. Ahmadi, *Microchem. J.*, 2019, **147**, 198–206.
65 M. Roushani, Z. Rahmati, S. Farokhi, S. J. Hoseini and R. H. Fath, *Mater. Sci. Eng., C*, 2020, **108**, 110388.
66 R. Nehru, C.-D. Dong and C.-W. Chen, *ACS Appl. Nano Mater.*, 2021, **4**, 6768–6777.
67 H. Mater Mahnashi, A. M. Mahmoud, A. Saad Alkahtani and M. M. El-Wekil, *Microchem. J.*, 2021, **163**, 105925.
68 K. Venkatesh, R. Rajakumaran, S. M. Chen, C. Karuppiah, C. C. Yang, S. K. Ramaraj, M. A. Ali, F. M. A. Al-Hemaid, M. S. El-Shikh and B. M. A. Almunqedhi, *Chemosphere*, 2021, **273**, 129665.
69 M. Lu, C. Cao, F. Wang and G. Liu, *Mater. Des.*, 2021, **199**, 109409.
70 Y. G. Zhu, X. F. Li, M. F. Wu, M. J. Shi, Q. C. Tian, L. Fu, H. S. Tsai, W. F. Xie, G. S. Lai, G. Wang, N. Jiang, C. Ye and C. T. Lin, *Anal. Chim. Acta*, 2023, **1275**, 341607.
71 J. Huang, Z. Qiu, J. Lin, J. Lin, F. Zhu, G. Lai and Y. Li, *Microchem. J.*, 2023, **188**, 108444.
72 P. Kolhe, A. Roberts and S. Gandhi, *Food Chem.*, 2023, **398**, 133846.
73 A. Wong, C. A. Razzino, T. A. Silva and O. Fatibello-Filho, *Sens. Actuators, B*, 2016, **231**, 183–193.
74 A. Kling, C. Chatelle, L. Armbrecht, E. Qelibari, J. Kieninger, C. Dincer, W. Weber and G. Urban, *Anal. Chem.*, 2016, **88**, 10036–10043.
75 T. M. Rawson, S. A. N. Gowers, D. M. E. Freeman, R. C. Wilson, S. Sharma, M. Gilchrist, A. MacGowan, A. Lovering, M. Bayliss, M. Kyriakides, P. Georgiou, A. E. G. Cass, D. O'Hare and A. H. Holmes, *Lancet Digital Health*, 2019, **1**, e335–e343.
76 S. Kumar, P. Karfa, K. C. Majhi and R. Madhuri, *Mater. Sci. Eng., C*, 2020, **111**, 110777.

77 J. Li and X. Bo, *J. Hazard. Mater.*, 2022, **423**, 127014.
78 R. Umapathi, S. M. Ghoreishian, S. Sonwal, G. M. Rani and Y. S. Huh, *Coord. Chem. Rev.*, 2022, **453**, 214305.
79 L. Qian, A. R. Thiruppathi, J. van der Zalm and A. Chen, *ACS Appl. Nano Mater.*, 2021, **4**, 3696–3706.
80 C. A. Donini, M. K. L. da Silva, R. P. Simões and I. Cesarino, *Electroanal. Chem.*, 2018, **809**, 67–73.
81 C. L. Malonga Matanou, B. R. Malonda-Boungou, M. N'Dollo, M. D. Nkoua Ngavouka, P. S. Moussounda, A. T. Raji and B. M'Passi-Mabiala, *J. Phys. Chem. Solids*, 2020, **138**, 109162.
82 A. R. Cardoso, A. C. Marques, L. Santos, A. F. Carvalho, F. M. Costa, R. Martins, M. G. F. Sales and E. Fortunato, *Biosens. Bioelectron.*, 2019, **124–125**, 167–175.
83 K. Abnous, N. M. Danesh, M. Ramezani, A. S. Emrani and S. M. Taghdisi, *Biosens. Bioelectron.*, 2016, **78**, 80–86.
84 L. Gao, Q. Mao, S. Luo, L. Cao, X. Xie, Y. Yang, Y. Deng and Z. Wei, *Environ. Pollut.*, 2020, **259**, 113795.
85 Q. He, B. Yu, Z. Li and Y. Zhao, *Energy Environ. Mater.*, 2019, **2**, 264–279.
86 X. Wu, F. Kang, W. Duan and J. Li, *Prog. Nat. Sci.*, 2019, **29**, 247–255.
87 X. Duan, H. Sun and S. Wang, *Acc. Chem. Res.*, 2018, **51**, 678–687.
88 P. Rebelo, J. G. Pacheco, I. V. Voroshylova, A. Melo, M. N. D. S. Cordeiro and C. Delerue-Matos, *Sens. Actuators, B*, 2021, **329**, 129112.
89 P. Zhang, Y. Yang, X. Duan, Y. Liu and S. Wang, *ACS Catal.*, 2021, **11**, 11129–11159.
90 M. K. L. Da Silva, R. Plana Simões and I. Cesarino, *Electroanalysis*, 2018, **30**, 2066–2076.
91 J. S. Won, J. Kaewsuk, J. H. Jo, D.-H. Lim and G. T. Seo, *J. Adv. Oxid. Technol.*, 2015, **18**, 31–38.
92 O. C. Adekoya, G. J. Adekoya, R. E. Sadiku, Y. Hamam and S. S. Ray, *ACS Omega*, 2022, **7**, 33808–33820.
93 A. O. Osikoya, F. Opoku and P. P. Govender, *Chem. Phys. Lett.*, 2021, **764**, 138278.
94 M. Ding, D. C. Sorescu and A. Star, *J. Am. Chem. Soc.*, 2013, **135**, 9015–9022.
95 X. Ren, H. Guo, J. Feng, P. Si, L. Zhang and L. Ci, *Chemosphere*, 2018, **191**, 389–399.
96 J. Moens, P. Jaque, F. De Proft and P. Geerlings, *J. Phys. Chem. A*, 2008, **112**, 6023–6031.
97 C. Ye, F. Zhang, X. Tan, H. F. Sun, W. Dai, K. Yang, M. H. Yang, S. Y. Du, D. Dai, J. H. Yu, N. Jiang, W. T. Su, L. Fu, H. Li, J. Kong and C. T. Lin, *Chin. Chem. Lett.*, 2020, **31**, 2507–2511.
98 X. Ding, H. Liu and Y. Fan, *Adv. Healthcare Mater.*, 2015, **4**, 1451–1468.
99 K. S. Novoselov, V. I. Fal'ko, L. Colombo, P. R. Gellert, M. G. Schwab and K. Kim, *Nature*, 2012, **490**, 192–200.
100 H. P. Bei, Y. Yang, Q. Zhang, Y. Tian, X. Luo, M. Yang and X. Zhao, *Molecules*, 2019, **24**, 658.
101 S. Ayyaru and Y. H. Ahn, *J. Membr. Sci.*, 2017, **525**, 210–219.
102 N. Golafshan, M. Kharaziha and M. Fathi, *Carbon*, 2017, **111**, 752–763.
103 K. Abnous, N. M. Danesh, M. Alibolandi, M. Ramezani, S. M. Taghdisi and A. S. Emrani, *Sens. Actuators, B*, 2017, **240**, 100–106.
104 F. Wang, L. H. Zhu and J. D. Zhang, *Sens. Actuators, B*, 2014, **192**, 642–647.
105 Y. Zhu, T. H. Liu, W. Zhou, M. Shi, M. Wu, P. Shi, N. Zhao, X. Li, Z. Zhang, D. Zhang, Y. Lv, W. Wu, H. S. Tsai, G. Lai, L. Fu, H. Karimi-Maleh, H. Li, N. Jiang, C. Ye and C. T. Lin, *Small Struct.*, 2024, **5**, 2400034.
106 Y. Zhu, X. Li, M. Wu, M. Shi, Q. Tian, L. Fu, H.-S. Tsai, W.-F. Xie, G. Lai, G. Wang, N. Jiang, C. Ye and C.-T. Lin, *Anal. Chim. Acta*, 2023, **1275**, 341607.
107 X. Hong, B. Zhang, E. Murphy, J. Zou and F. Kim, *J. Power Sources*, 2017, **343**, 60–66.
108 M. Xu, Y. Zhu, S. Gao, Z. Zhang, Y. Gu and X. Liu, *ACS Appl. Nano Mater.*, 2021, **4**, 12442–12452.
109 T.-K. Hong, D. W. Lee, H. J. Choi, H. S. Shin and B.-S. Kim, *ACS Nano*, 2010, **4**, 3861–3868.
110 X. Wang, J. Wang, H. Cheng, P. Yu, J. Ye and L. Mao, *Langmuir*, 2011, **27**, 11180–11186.
111 U. Han, Y. Seo and J. Hong, *Sci. Rep.*, 2016, **6**, 24158.
112 F.-X. Xiao, J. Miao and B. Liu, *J. Am. Chem. Soc.*, 2014, **136**, 1559–1569.
113 Q. Yuan, Y. Liu, C. Ye, H. Sun, D. Dai, Q. Wei, G. Lai, T. Wu, A. Yu, L. Fu, K. W. A. Chee and C.-T. Lin, *Biosens. Bioelectron.*, 2018, **111**, 117–123.
114 H. Chen, X. Wu, R. Zhao, Z. Zheng, Q. Yuan, Z. Dong and W. Gan, *Mikrochim. Acta*, 2019, **186**, 623.
115 N. Sebastian, W.-C. Yu and D. Balram, *Inorg. Chem. Front.*, 2019, **6**, 82–93.
116 H. Teymourian, M. Parrilla, J. R. Sempionatto, N. F. Montiel, A. Barfidokht, R. Van Echelpoel, K. De Wael and J. Wang, *ACS Sens.*, 2020, **5**, 2679–2700.
117 S. A. N. Gowers, D. M. E. Freeman, T. M. Rawson, M. L. Rogers, R. C. Wilson, A. H. Holmes, A. E. Cass and D. O'Hare, *ACS Sens.*, 2019, **4**, 1072–1080.
118 J. Tu, R. M. Torrente-Rodríguez, M. Wang and W. Gao, *Adv. Funct. Mater.*, 2019, **30**, 1906713.
119 S. Eyvazi, B. Baradaran, A. Mokhtarzadeh and M. D. L. Guardia, *Trends Food Sci. Technol.*, 2021, **114**, 712–721.
120 H. Sohrabi, A. Hemmati, M. R. Majidi, S. Eyvazi, A. Jahanban-Esfahlan, B. Baradaran, R. Adlpour-Azar, A. Mokhtarzadeh and M. de la Guardia, *TrAC, Trends Anal. Chem.*, 2021, **143**, 116344.
121 H. M. Mohamed, *TrAC, Trends Anal. Chem.*, 2016, **82**, 1–11.
122 L. Fu, Y. Zheng, P. Zhang, H. Zhang, Y. Xu, J. Zhou, H. Zhang, H. Karimi-Maleh, G. Lai, S. Zhao, W. Su, J. Yu and C. T. Lin, *Biosens. Bioelectron.*, 2020, **159**, 112212.
123 R. K. Mishra, L. J. Hubble, A. Martin, R. Kumar, A. Barfidokht, J. Kim, M. M. Musameh, I. L. Kyratzis and J. Wang, *ACS Sens.*, 2017, **2**, 553–561.
124 P. A. Raymundo-Pereira, N. O. Gomes, F. M. Shimizu, S. A. S. Machado and O. N. Oliveira, *Chem. Eng. J.*, 2021, **408**, 127279.
125 J. A. Roberts, M. H. Abdul-Aziz, J. Lipman, J. W. Mouton, A. A. Vinks, T. W. Felton, W. W. Hope, A. Farkas,

M. N. Neely, J. J. Schentag, G. Drusano, O. R. Frey, U. Theuretzbacher and J. L. Kuti, *Lancet Infect. Dis.*, 2014, **14**, 498–509.

126 L. C. Tai, W. Gao, M. Chao, M. Bariya, Q. P. Ngo, Z. Shahpar, H. Y. Y. Nyein, H. Park, J. Sun, Y. Jung, E. Wu, H. M. Fahad, D. H. Lien, H. Ota, G. Cho and A. Javey, *Adv. Mater.*, 2018, **30**, e1707442.

127 R. K. Mishra, K. Y. Goud, Z. Li, C. Moonla, M. A. Mohamed, F. Tehrani, H. Teymourian and J. Wang, *J. Am. Chem. Soc.*, 2020, **142**, 5991–5995.

128 H. C. Ates, H. Mohsenin, C. Wenzel, R. T. Glatz, H. J. Wagner, R. Bruch, N. Hoefflin, S. Spassov, L. Streicher, S. Lozano-Zahonero, B. Flamm, R. Trittler, M. J. Hug, M. Kohn, J. Schmidt, S. Schumann, G. A. Urban, W. Weber and C. Dincer, *Adv. Mater.*, 2022, **34**, e2104555.

129 J. Zhang, Z. Yang, Q. Liu and H. Liang, *Talanta*, 2019, **202**, 384–391.

130 A. Hrioua, A. Loudiki, A. Farahi, M. Bakasse, S. Lahrich, S. Saqrane and M. A. El Mhammedi, *Bioelectrochemistry*, 2021, **137**, 107687.

131 N. Sharma, S. Panneer Selvam and K. Yun, *Appl. Surf. Sci.*, 2020, **512**, 145742.

132 W. Yi, Z. Li, C. Dong, H.-W. Li and J. Li, *Microchem. J.*, 2019, **148**, 774–783.

133 M. Behravan, H. Aghaie, M. Giahi and L. Maleknia, *Diamond Relat. Mater.*, 2021, **117**, 108478.

134 S. Chinnaraj, V. Palani, S. Yadav, M. Arumugam, M. Sivakumar, V. Maluventhen and M. Singh, *Sens. Bio-Sens. Res.*, 2021, **32**, 100425.

135 Y. Yuan, X. Xu, J. Xia, F. Zhang, Z. Wang and Q. Liu, *Mikrochim. Acta*, 2019, **186**, 191.

136 A. A. Ensafi, M. Sohrabi, M. Jafari-Asl and B. Rezaei, *Appl. Surf. Sci.*, 2015, **356**, 301–307.

137 B. Y. Zhao, Q. Wei, C. Xu, H. Li, D. Wu, Y. Cai, K. Mao, Z. Cui and B. Du, *Sens. Actuators, B*, 2011, **155**, 618–625.

138 M. Hu, X. Hu, Y. Zhang, M. Teng, R. Deng, G. Xing, J. Tao, G. Xu, J. Chen, Y. Zhang and G. Zhang, *Sens. Actuators, B*, 2019, **288**, 571–578.

139 A. Benvidi, M. D. Tezerjani, S. M. Moshtaghiun and M. Mazloum-Ardakani, *Microchim. Acta*, 2016, **183**, 1797–1804.